Legendre fit to $p(\vec{e}, e'\vec{p})\pi^0$ response functions at $Q^2 = 1$ (GeV/c)^2 across the $\Delta(1232)$ resonance

Internal Report to the JLab E91-011 Collaboration

J. J. Kelly[1]

[1]*Department of Physics, University of Maryland, College Park, Maryland 20742, USA*

(Dated: April 12, 2005; revised July 18, 2005)

Legendre fits were made to JLab e91011 cross section and response function data for $p(\vec{e}, e'\vec{p})\pi^0$ at $Q^2 = 1.0$ (GeV/c)^2 with $1.17 \le W \le 1.35$ GeV in 10 bins across the $\Delta(1232)$ resonance. The sensitivity of the data to terms beyond the customary *sp* truncation is examined and comparisons are made with representative models.

I. INTRODUCTION

This internal report presents some of the details for the Legendre analysis of data for the differential cross section and recoil-polarization response functions for the $p(\vec{e}, e'\vec{p})\pi^0$ reaction at $Q^2 = 1.0$ (GeV/c)^2 across the $\Delta(1232)$ resonance that were obtained by the JLab e91011 collaboration. This report is updated periodically as the analysis evolves. The final version is intended as a supplement to a Phys. Rev. C paper [1] because there are far too many figures for a typical journal paper. Details of the conventions for response functions are presented in the PRC draft and will not be repeated here. Some of the present figures are too cluttered for final publication but contain useful information about intermediate stages of the analysis that is worth preserving nonetheless. The PRC paper will include more streamlined versions of selected figures from this and similar reports, along with a more detailed and integrated discussion of the physics conclusions.

Three fits were made for each binning scheme, insightfully designated A, B, and C. Fit A, the simplest, uses *sp* truncation and the assumption of M_{1+} dominance to limit the number of Legendre coefficients for each response functions. Although this truncation scheme provides satisfactory results for most response functions, for some responses good fits in the middle of the (W, Q^2) acceptance clearly require 1 or 2 additional terms. Hence, Fit B was made using additional terms for any response function that appears to need them in any (W, Q^2) bin. For this version the number of coefficients in each response function was independent of (W, Q^2) bin. However, because these additional terms were sometimes insufficiently constrained, one finds large uncertainties in fitted quantities and strong correlations among parameters for bins near the edges of the acceptance. Therefore, the final analysis, Fit C, adjusted the number of parameters for each bin separately based upon *sp* truncation at the edges and greater flexibility in the middle of the acceptance. Neighboring bins were sometimes considered also, to minimize the frequency of changes in the number of degrees of freedom. Although the criteria for Fit C are more subjective, the results should be the more stable than Fit B and more reliable than Fit A.

II. METHODS

A. Data selection

The data consist of differential cross sections and beam analyzing powers binned in (W, Q^2, x_{cm}, ϕ) and recoil-polarization response functions binned in (W, Q^2, x_{cm}), where W is invariant mass, Q^2 is photon virtuality, and $x_{cm} = \cos\theta_{cm}$ and ϕ are determined by the pion polar and azimuthal angles in the πN center of mass frame relative to the momentum transfer $\vec{q}$ and the electron scattering plane. A cut on $Q^2 = 1.0 \pm 0.2$ (GeV/c)^2 was used for all quantities and 10 bins of width ± 0.1 GeV span the Δ resonance, $1.17 \le W \le 1.35$ GeV, but the central region, defined by $1.21 \le W \le 1.29$ GeV, offers the most complete angular coverage. Differential cross section and beam analyzing power data were projected to central kinematics for each (W, Q^2, x_{cm}, ϕ) using the MAID2000 model [2] and are presented on uniform grids with $x_k = -0.95 + 0.10 * k, k = 1, 20$ and $\phi_k = 15° + 30° * k, k = 1, 12$. See Ref. [3] for details of the cross section analysis. Data for recoil-polarization response functions employed a nonuniform grid designed to obtain approximately uniform statistical precision. Hence, bin widths are smaller for negative than for positive x_{cm}. Those data have not been projected to central kinematics. Therefore, the Legendre fit uses acceptance-averaged values for x_{cm} and a projection procedure for the Q^2 dependence that is described in the next section.

For display purposes we often show response functions for the unpolarized cross section and beam analyzing power deduced from the ϕ dependence of those data, but the Legendre analysis uses the original data binned in ϕ rather than the corresponding response functions. Note that for some polar angles the azimuthal acceptance is not sufficient for extraction of unpolarized response functions and one cannot separate R_{LT} and R_{TT} from R_{L+T}; nevertheless, the differential cross section data retain some sensitivity to the Legendre coefficients for those response functions even where some of the angular distributions become sparse.

B. Projection to nominal Q^2

Acceptance averaging results in significant variations of Q^2 with respect to x_{cm} and W. Let $\overline{Q^2}$ represent the acceptance-averaged Q^2 for a specified (W, x_{cm}) bin. For a given W, nonmonotonic variations of $\overline{Q^2}$ with respect to x_{cm} increase the scatter in response functions and may artificially enhance high-order Legendre coefficients fit to their angular distributions. [15] Consequently, it is useful to project the response function data to the nominal $Q^2 = 1.0$ (GeV/c)^2 for the experiment before fitting angular distributions. The cross section analysis already compensates for small kinematical variations by comparing acceptance-averaged cross sections for Monte Carlo calculations with model cross sections for central kinematics, but this type of analysis has not been attempted for recoil polarization because none of the available models provides a sufficiently good description of those data. Furthermore, it is not clear that ratios of averaged and central calculations provide the most reliable corrections for response functions with nodes. A comparison of several prescriptions for kinematical corrections was made in a similar report on the multipole analysis [4] where it was concluded that scaling according to a common dipole form factor is sufficient. The kinematical shifts are relatively small and errors due to uncertainties in the projection procedure should tend to average out when fitting angular distributions. Therefore, we project response functions to nominal Q^2 according to

$$R(x, W, Q_0^2) = R(x, W, \overline{Q^2}) \left(\frac{1 + \overline{Q^2}/\Lambda^2}{1 + Q_0^2/\Lambda^2} \right)^4 \tag{1}$$

where $\Lambda^2 = 0.71$ (GeV/c)^2 is the traditional dipole scale and where $Q_0^2 = 1.0$ (GeV/c)^2 represents central kinematics for e91011.

C. Systematic errors

Although some of the systematic uncertainties that affect response functions vary with spectrometer settings, beam conditions, and time, those variations are expected to be small compared to either statistical uncertainties or average total systematic uncertainty. Therefore, we believe that it is sufficient to perform a more schematic analysis of the propagation of errors. Our basic strategy is to evaluate the sensitivity of fitted Legendre coefficients to small variations of various calibration scales or to corrections for background, false asymmetry, or acceptance averaging. For example, the systematic uncertainty due to FPP analyzing power is treated as a scale uncertainty common to all recoil-polarization response functions and their corresponding Legendre coefficients and we do not consider separate variations for each analyzer thickness or momentum setting, which would require many replays. Similarly, the uncertainties due to false asymmetry are estimated to be a fraction of the difference between Legendre coefficients fitted to data obtained with or without inclusion of false asymmetry in the likelihood function used in replay.

Let $y(\lambda_i)$ represent a quantity, such as a quadrupole ratio or Legendre coefficient, fitted to a data set for which one of the scale factors has the value λ_i. The net systematic error then takes the form

$$(\delta y)^2_{\rm sys} = \sum_i \left(\frac{\partial y}{\partial \lambda_i} \delta\lambda_i \right)^2 = \sum_i \left(y(\lambda_i + \delta\lambda_i) - y(\lambda_i) \right)^2 \tag{2}$$

where most scale factors would have nominal values of $\lambda_i = 1$. Dependencies on fixed parameters are suppressed.

The following systematic effects will be considered. More details about the methods for evaluating systematic uncertainties and the sensitivity of response functions to these sources of systematic error can be found in Ref. [5].

normalization: a common normalization uncertainty for differential cross sections and response functions

beam polarization: the systematic relative uncertainty for Compton measurements of beam polarization is estimated to be about 1.4% [6]

analyzing power: the relative uncertainties in average analyzing power reported by Punjabi *et al.*[7] are in the $1-2\%$ range. Because we do not consider thickness or momentum variations, we adopt a fairly conservative estimate of $\delta A_y/A_y = 0.02$.

elastic subtraction: the correction for elastic contamination is small and only affects bins with $x_{cm} = -0.15$ and 0.2, but the contamination fractions binned in ϕ were difficult to determine. Therefore, we estimated the systematic uncertainty due to elastic contamination using a relative uncertainty of 100% in its scale factor. The effect on fitted Legendre coefficients and quadrupole ratios remains negligible despite this generous uncertainty.

false asymmetry: the systematic uncertainty due to the corrections for false asymmetry are estimated by comparing fits to data replayed with and without false asymmetry. We assume that the relative uncertainty in false asymmetry is approximately 10%.

spin rotation: the systematic uncertainties due to spin rotation are analyzed using a simplified geometric model based containing 6 parameters. Uncertainties due to each of these parameters are evaluated by comparing replays with modified and nominal values for those angles. We use the same uncertainties in the spin rotation parameters and angle reconstructions that were reported in Refs. [7, 8].

bin centering: the variation of acceptance-averaged Q^2 with x_{cm} is compensated for the recoil-polarization response functions using a dipole form factor. The uncertainty due to the choice of form factor is estimated by comparison with fits using the Sato-Lee parameterization [9] of the $N \to \Delta$ form factor instead.

D. Legendre expansions

Each of the response functions can be represented by a Legendre expansion of the form

$$R_\eta(x, W, Q^2) = \sum_{n=0}^{N_\eta} A_n^\eta(W, Q^2) P_n(x) \tag{3}$$

where η represents all of the labels needed to identify a particular response function and N_η is the maximum order employed. Each of the Legendre coefficients can be further expanded in terms of products of pairs of multipole amplitudes, but these expansions quickly become unwieldy as the number of participating partial waves increases. Analyses of previous data for differential cross section have usually found that fits using truncated Legendre expansions based upon M_{1+} dominance describe the data well in the immediate vicinity of the Δ resonance. Tables I-III display truncated expansions that are limited to s and p waves and that require M_{1+} to appear in every term. To streamline the notation, each coefficient is obtained from either the real or imaginary part of $M_{1+}^* B_{\eta n}$ where the phase type is indicated in the second column and $B_{\eta n}$ is listed in the fourth column of these tables. The last column gives the response-function labels that will appear in multipanel figures.

The Legendre coefficients $A_n^\eta(W, Q^2)$ are obtained by fitting response-function and/or cross section angular distributions for each (W, Q^2). The simplest fits, which we label Fit A, truncate the expansion for R_η at the order, N_η, suggested by the *sp* model with M_{1+} dominance. For some response functions, good fits to the data for several of the central W bins require an additional term or two beyond *sp* truncation. Thus, Fit B employs a larger number of free parameters but the number of parameters does not vary with W. Finally, Fit C optimizes N_η for three ranges of W — large enough to obtain good fits for central W, but smaller for either low or high W where the angular coverage cannot constrain as many terms.

TABLE I: Truncated Legendre expansion of the differential cross section. Legendre coefficients based upon the assumption of M_{1+} dominance are obtained as either the real or imaginary parts of $M_{1+}^{*}B_{\eta,n}$. The final column lists the labels used in figures.

R_η	type	n	$B_{\eta,n}$	label
R_L	Re	0		
R_T	Re	0	$2M_{1+}$	L+T(0)
		1	$2E_{0+}$	
		2	$-M_{1+}+6E_{1+}-2M_{1-}$	
R_{TT}	Re	0	$-\frac{3}{2}M_{1+}-3E_{1+}-3M_{1-}$	TT(0)
R_{LT}	Re	0	S_{0+}	LT(0)
		1	$6S_{1+}$	
R'_{LT}	Im	0	S_{0+}	LTh(0)
		1	$6S_{1+}$	

TABLE II: Truncated Legendre expansion of the helicity-dependent recoil polarization. Legendre coefficients based upon the assumption of M_{1+} dominance are obtained as either the real or imaginary parts of $M_{1+}^{*}B_{\eta,n}$.

R_η	type	n	$B_{\eta,n}$	label
R'^{n}_{LT}	Re	0	S_{1-}	LThn
		1	S_{0+}	
		2	$4S_{1+}$	
R'^{ℓ}_{LT}	Re	0	$-2(S_{1-}+S_{1+})$	LThl
		1	$-3S_{0+}$	
	Re	2	$-12S_{1+}$	
R'^{t}_{LT}	Re	0	$-S_{0+}$	LTht
		1	$S_{1-}-\frac{16}{5}S_{1+}$	
		2	$2S_{0+}$	
		3	$\frac{36}{5}S_{1+}$	
R'^{ℓ}_{TT}	Re	1	$-M_{1+}+\frac{6}{5}E_{1+}+2M_{1-}$	TThl
		2	$2E_{0+}$	
		3	$-\frac{36}{5}E_{1+}$	
R'^{t}_{TT}	Re	0	$-2M_{1+}+M_{1-}$	TTht
		1	$-3E_{0+}$	
		2	$-12E_{1+}$	

Terms beyond those in Tables I-III could arise from contributions with $\ell_\pi \geq 2$ or from terms that do not involve M_{1+}. Distinguishing between those possibilities is beyond the purview of Legendre analysis and requires a more fundamental multipole analysis instead. That type of analysis performed in Ref. [4]. Also note that this simple truncation suggests that some pairs of Legendre coefficients for different response functions are very closely related. However, a detailed examination shows that these simple relationships are often violated, again indicating failure of at least one of the assumptions of the simplest truncation scheme. A more detailed discussion of those issues is provided in the final paper [1] comparing Legendre and multipole fits. Here our objective is limited to a presentation of the three Legendre fits and evaluation of systematic uncertainties.

III. RESULTS

A. Cross section

The ϕ dependence of differential cross section in each (W, Q^2, x) bin is shown in Figs. 1 - 10. Each panel is labelled by x_{cm}. Differential cross sections were projected to nominal kinematics for each bin using the MAID2000 model [2]. The error bars include both statistical and bin-dependent systematic uncertainties, of which the sensitivity to the acceptance cut is usually dominant [3]. Dashed curves show Fit A, the *sp* truncation, while solid curves show Fit C with the number of terms adjusted according to the angular

TABLE III: Truncated Legendre expansion of the helicity-independent recoil polarization. Legendre coefficients based upon the assumption of M_{1+} dominance are obtained as either the real or imaginary parts of $M^*_{1+}B_{\eta,n}$.

R_η	type	n	$B_{\eta,n}$	label
R^n_L	Im		0	
R^n_T	Im	0	$-E_{0+}$	L+Tn
		1	$3M_{1-}$	
R^n_{LT}	Im	0	$-S_{1-}$	LTn
		1	$-S_{0+}$	
		2	$-4S_{1+}$	
R^ℓ_{LT}	Im	0	$-2(S_{1-}+S_{1+})$	LTl
		1	$-3S_{0+}$	
		2	$-12S_{1+}$	
R^t_{LT}	Im	0	$-S_{0+}$	LTt
		1	$S_{1-}-\frac{16}{5}S_{1+}$	
		2	$2S_{0+}$	
		3	$\frac{36}{5}S_{1+}$	
R^n_{TT}	Im	0	$3E_{0+}$	TTn
		1	$12E_{1+}-3M_{1-}$	
R^ℓ_{TT}	Im	0	$3E_{0+}$	TTl
		1	$18E_{1+}$	
R^t_{TT}	Im	0	$3M_{1-}$	TTt
		1	$-3E_{0+}$	
		2	$-12E_{1+}$	

coverage for each W. Although both Fits A and C reproduce the data well, the more detailed examination of Legendre coefficients presented in Sec. III B clearly shows that an additional term beyond *sp* truncation is warranted for both R_{LT} and R_{TT} in the central W region, $1.21 \leq W \leq 1.29$ GeV, where the angular coverage is most complete. It is important to recognize that Legendre fits use all of the cross section data for a given (W, Q^2) bin simultaneously; consequently, it is possible to obtain reasonable predictions for regions in (x_{cm}, ϕ) for which there are no data.

In addition, the dotted curves show fits to the ϕ distribution used to extract unpolarized response functions for each x_{cm}. These fits include 3 parameters for each x_{cm} panel in which there is sufficient ϕ coverage to separate R_{LT} and R_{TT} from R_{L+T}. Thus, there are potentially 45 free parameters for each (W, Q^2) compared with no more than 8 for Fit C. Consequently, the dotted curves occassionally become unphysical where the ϕ coverage is sparse while the Legendre fits remain reasonable. Of course, the uncertainties in the fitted cross sections expand in angular regions without data.

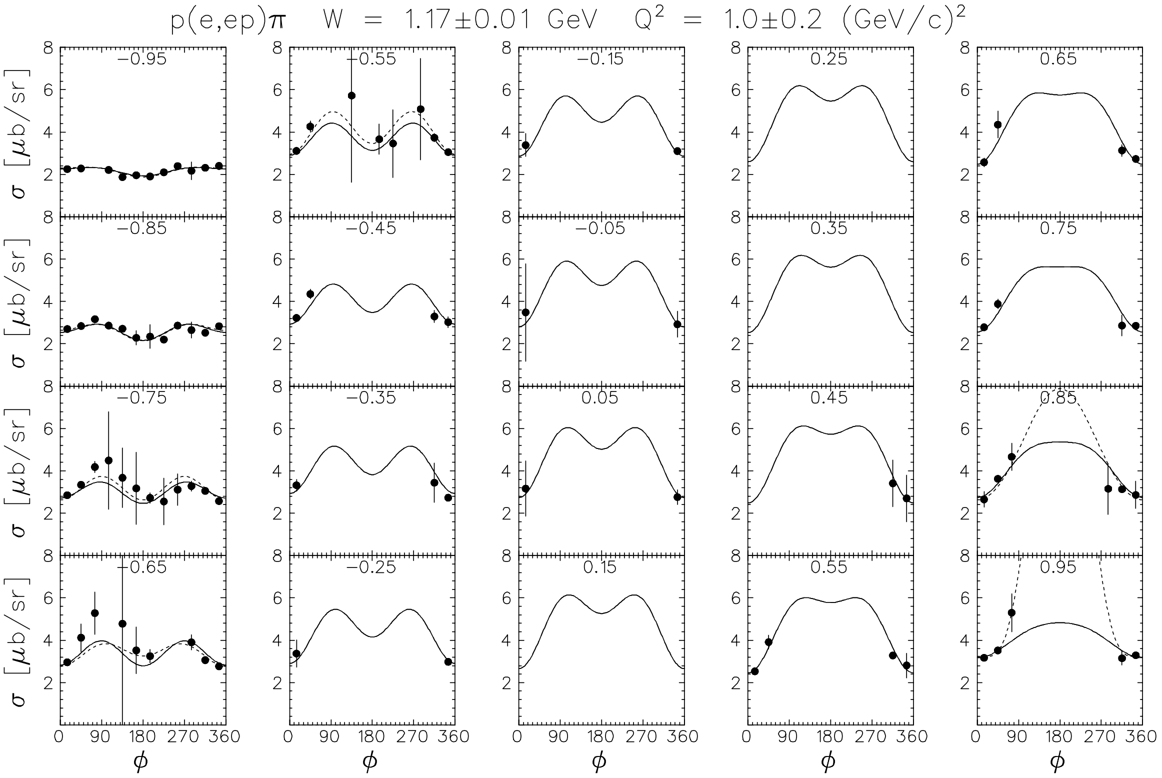

FIG. 1: Legendre fits to differential cross section for $W = 1.17$ GeV at $Q^2 = 1.0$ (GeV/c)^2. Dashed curves show Fit A while solid curves show Fit C. Dotted curves fit response functions to the ϕ dependence. See text for details.

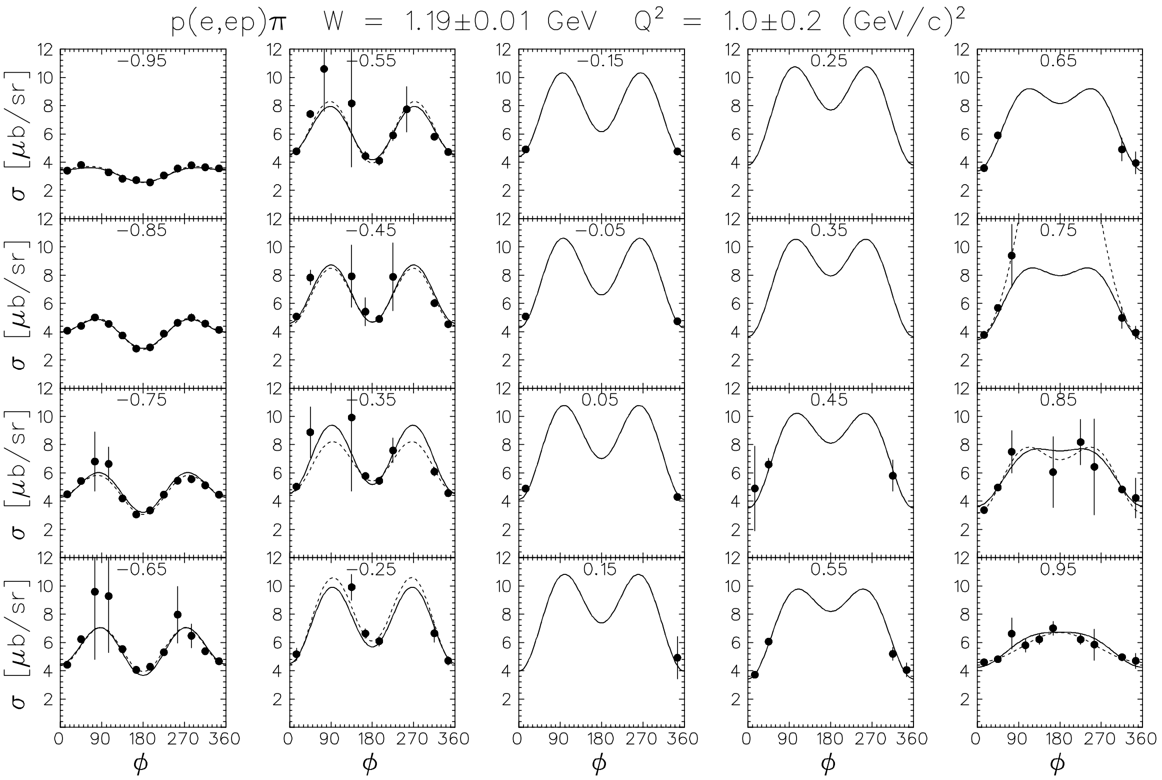

FIG. 2: Legendre fits to differential cross section for $W = 1.19$ GeV at $Q^2 = 1.0$ (GeV/c)^2. See Fig. 1 for the legend.

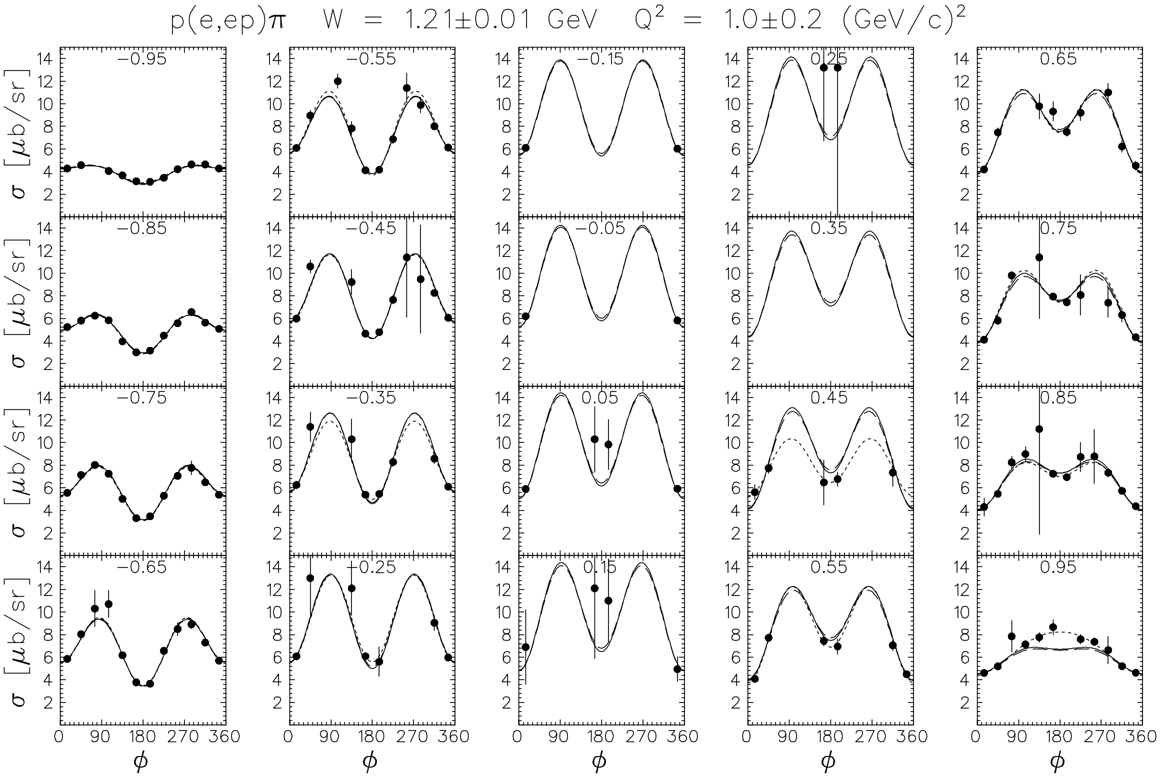

FIG. 3: Legendre fits to differential cross section for $W = 1.21$ GeV at $Q^2 = 1.0$ (GeV/c)^2. See Fig. 1 for the legend.

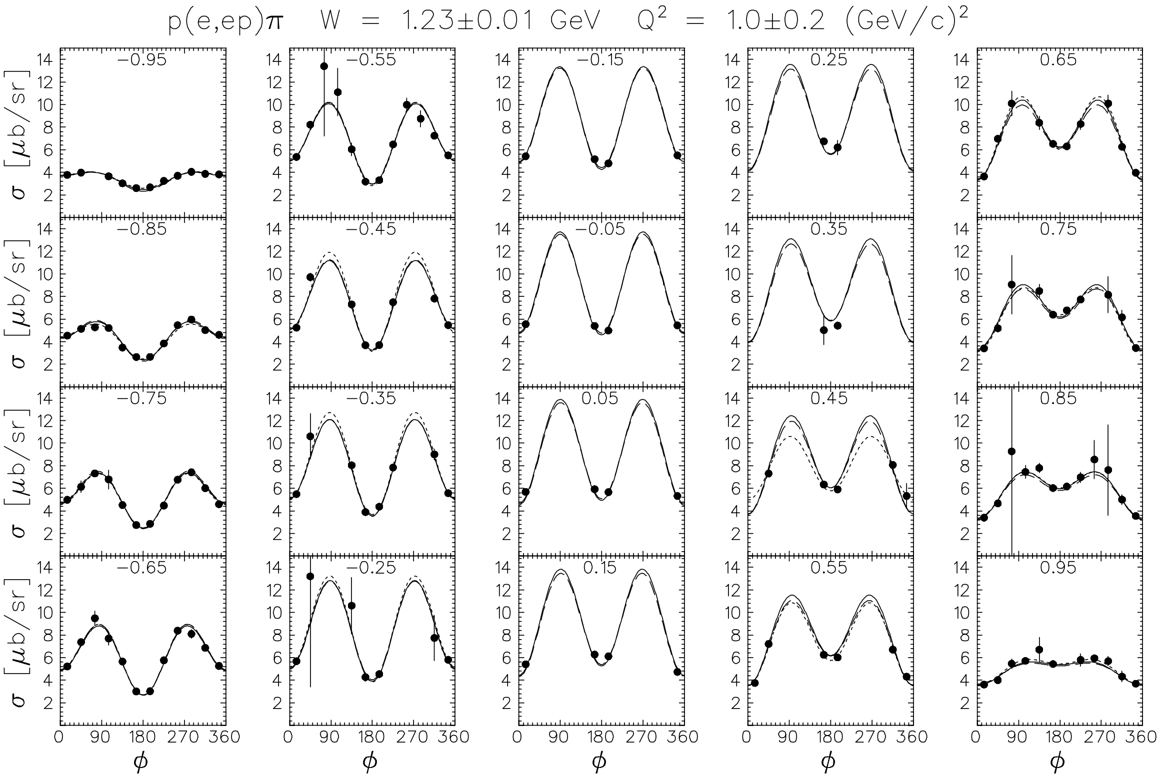

FIG. 4: Legendre fits to differential cross section for $W = 1.23$ GeV at $Q^2 = 1.0$ (GeV/c)^2. See Fig. 1 for the legend.

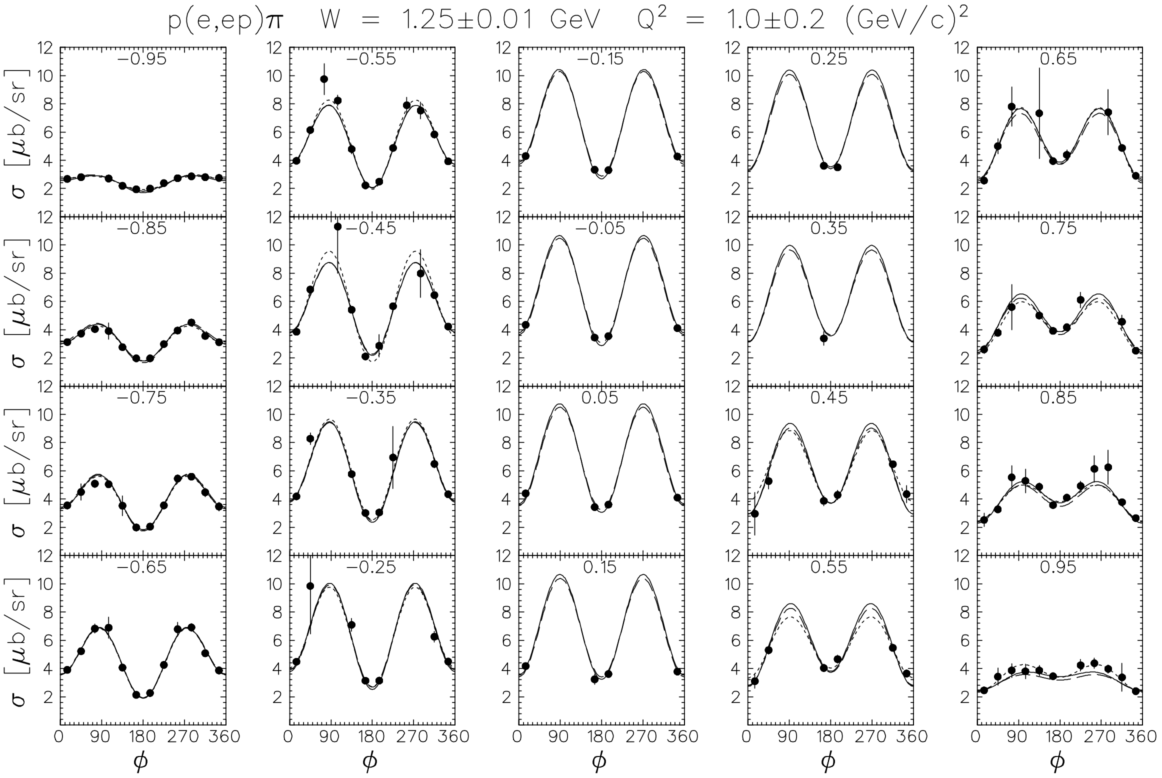

FIG. 5: Legendre fits to differential cross section for $W = 1.25$ GeV at $Q^2 = 1.0$ (GeV/c)^2. See Fig. 1 for the legend.

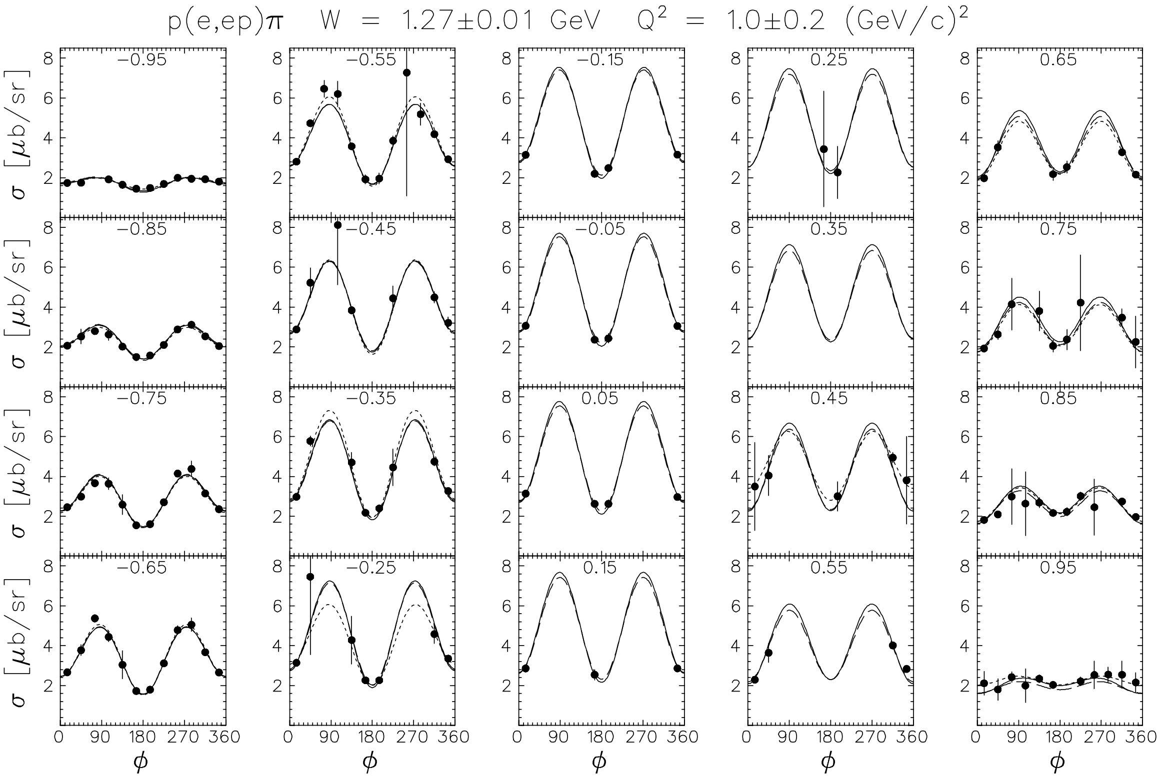

FIG. 6: Legendre fits to differential cross section for $W = 1.27$ GeV at $Q^2 = 1.0$ (GeV/c)^2. See Fig. 1 for the legend.

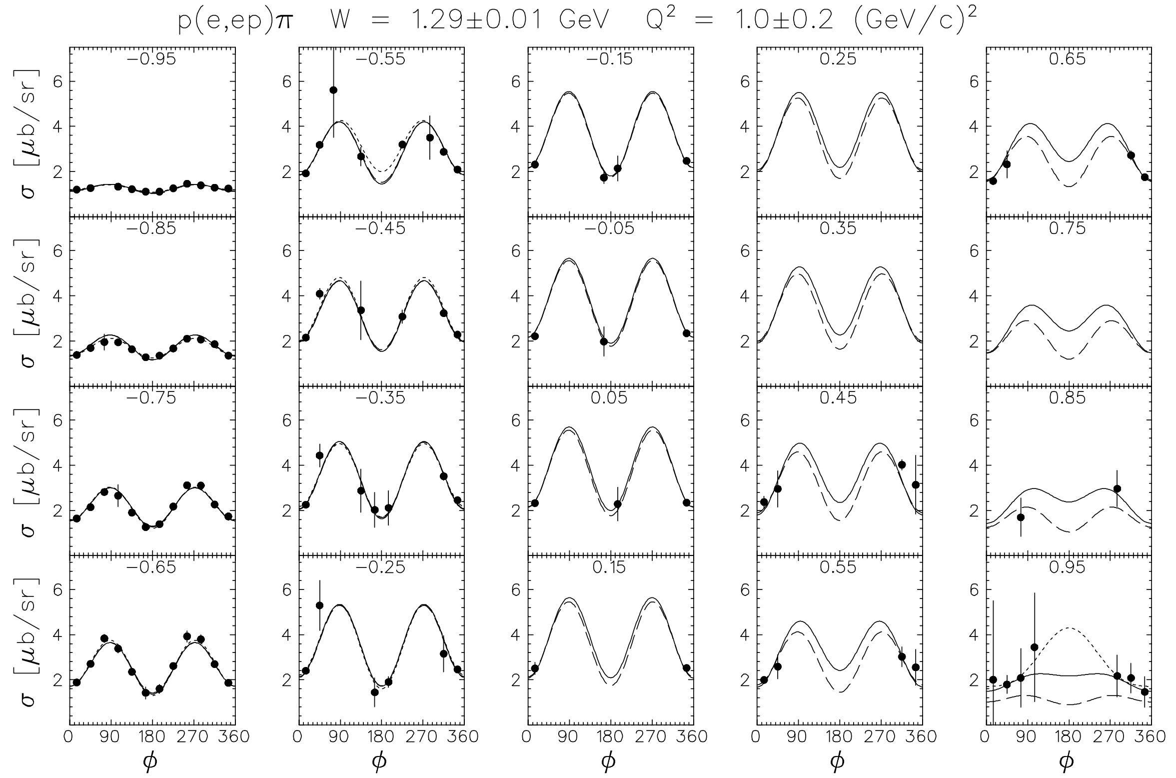

FIG. 7: Legendre fits to differential cross section for $W = 1.29$ GeV at $Q^2 = 1.0$ (GeV/c)^2. See Fig. 1 for the legend.

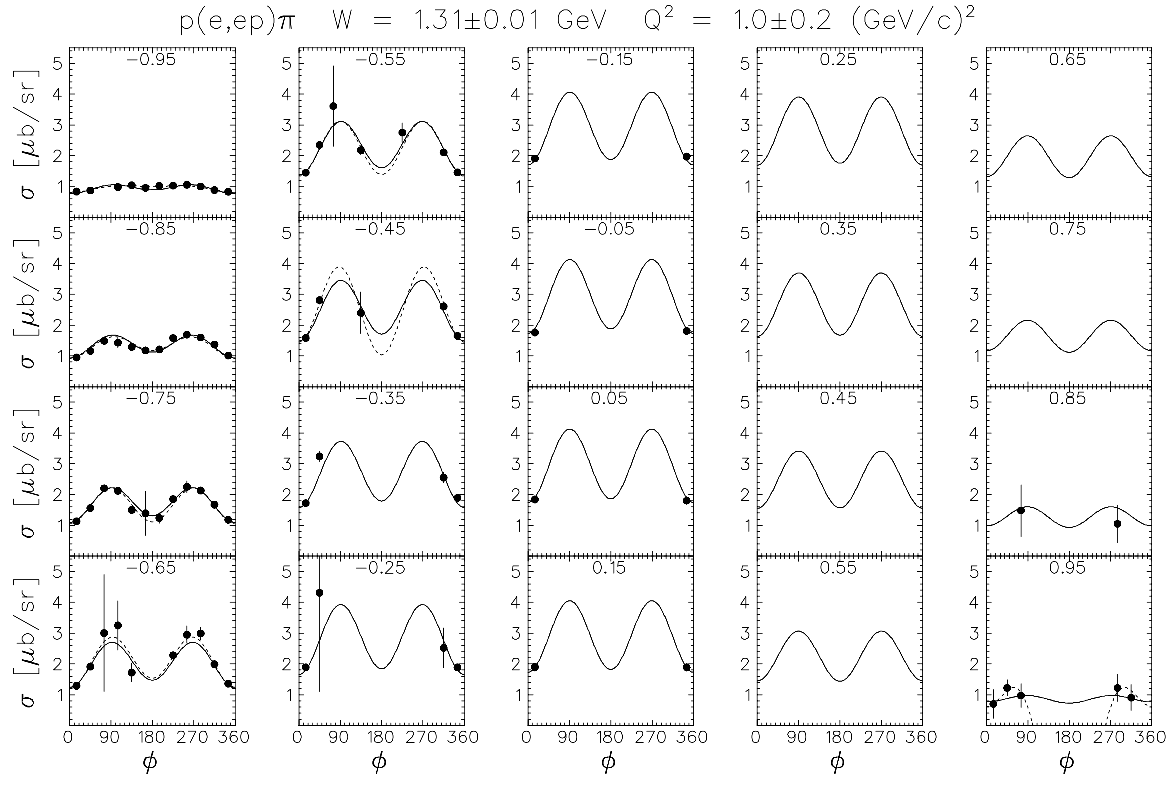

FIG. 8: Legendre fits to differential cross section for $W = 1.31$ GeV at $Q^2 = 1.0$ (GeV/c)^2. See Fig. 1 for the legend.

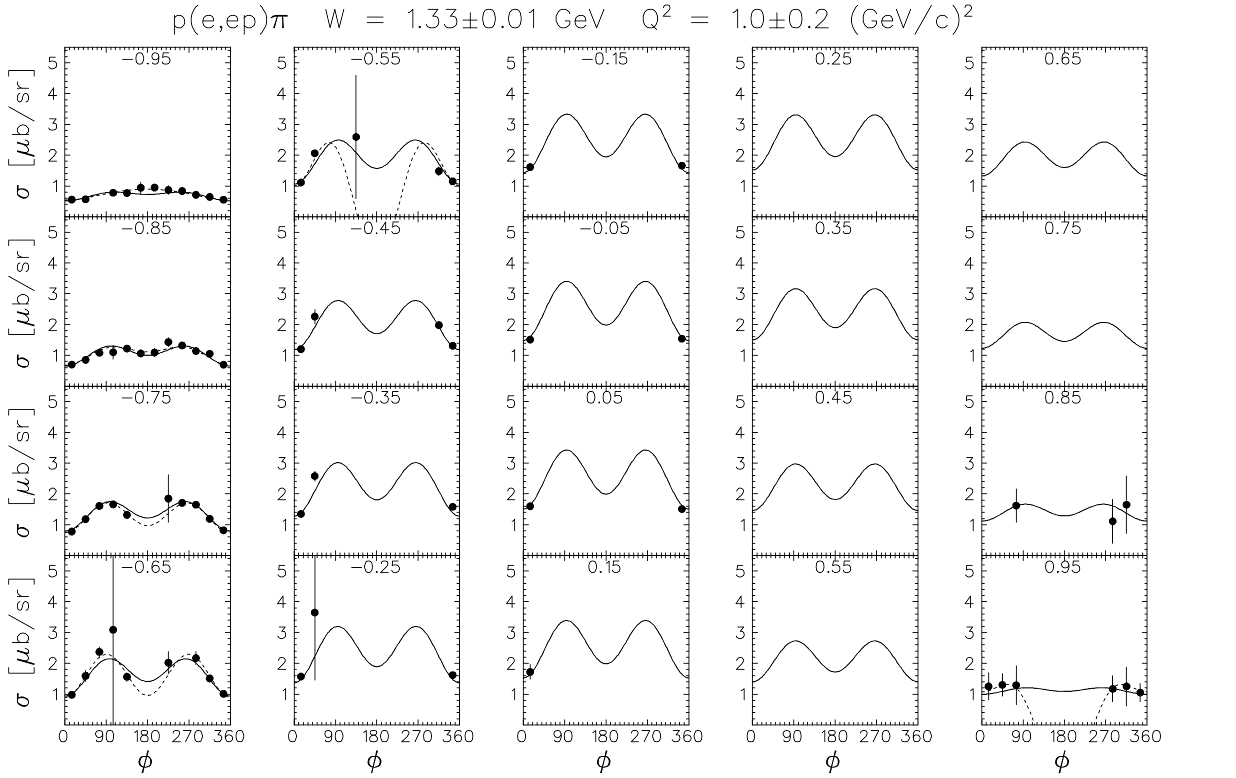

FIG. 9: Legendre fits to differential cross section for $W = 1.33$ GeV at $Q^2 = 1.0$ (GeV/c)^2. See Fig. 1 for the legend.

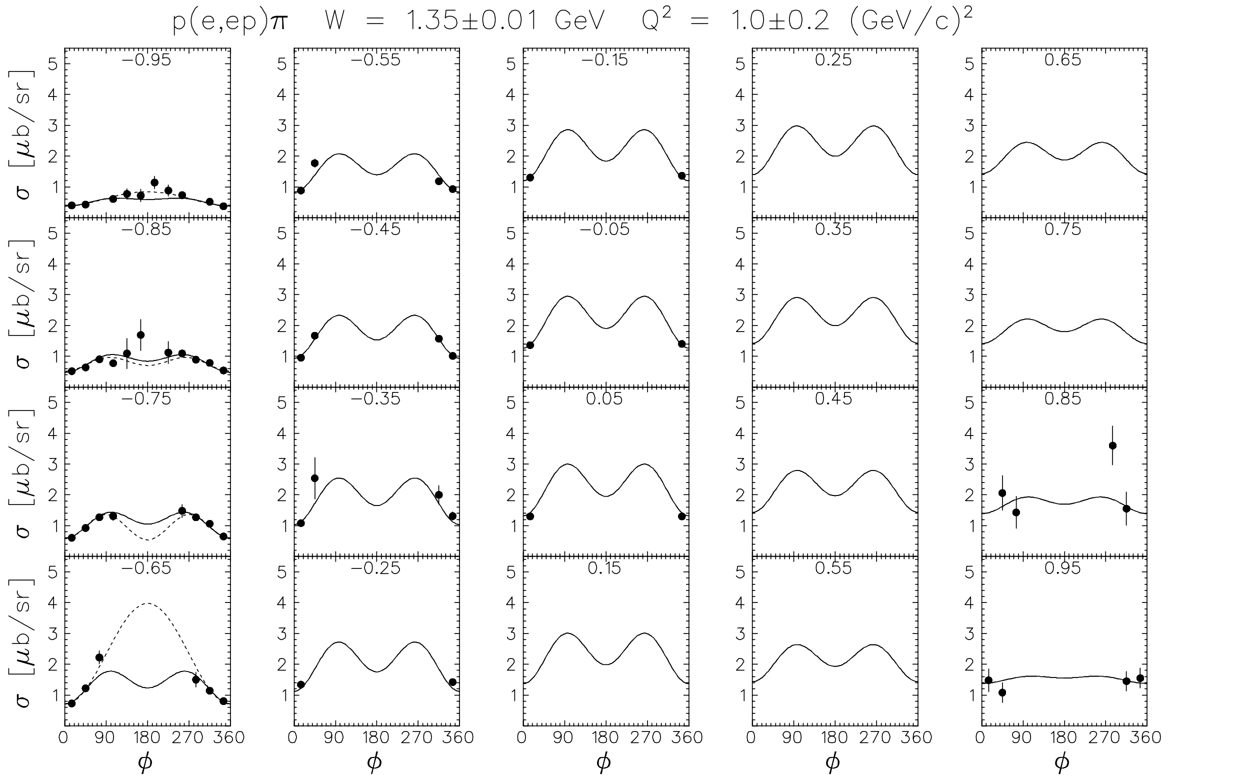

FIG. 10: Legendre fits to differential cross section for $W = 1.35$ GeV at $Q^2 = 1.0$ (GeV/c)^2. See Fig. 1 for the legend.

B. Response functions

Legendre fits to the response functions are shown in Figs. 11-20. The recoil-polarization data were projected to the nominal $Q^2 = 1.0$ (GeV/c)^2 using the dipole form factor and are plotted at acceptance-averaged values of x_{cm}. The Legendre coefficients were fit to the data in this form. In these figures, inner error bars with endcaps show statistical uncertanties while outer error bars without endcaps show total uncertainties for the recoil-polarization response functions that include systematic contributions accumulated in quadrature. However, the systematic contributions are visible only in the central W region where the statistical uncertainties are smallest. The systematic uncertainties are generally quite small and are dominated by normalization uncertainties in cross section, FPP analyzing power, and beam polarization which together are about $\pm3.6\%$ for helicity-independent or $\pm3.9\%$ for helicity-dependent response functions. The error bars for unpolarized and R'_{LT} response functions are not decomposed because those quantities were fit to data that include systematic uncertainties.

The dashed curves (Fit A) employ the *sp* truncation with M_{1+} dominance while solid curves (Fit C) permit one or two additional coefficients to vary for some of the response functions. The Legendre coefficients for R_{L+T}, R_{LT}, and R_{TT} were fit to the data for the differential cross section instead of to the response functions themselves. For some $x_{\rm cm}$ values the ϕ coverage was too limited for extraction of unpolarized response functions; consequently, fewer response data are shown than cross section data were fit. Nevertheless, the cross section data retain some sensitivity to Legendre coefficients for R_{L+T}, R_{LT}, and R_{TT} even when a response function decomposition is not possible for all angles.

All three curves are present in each panel, but the colored curved are often obscured by the solid black curves representing the final fits in which the number of terms for each response function is chosen by somewhat subjective criteria. In the central W region it is clear that good fits to some response functions require additional terms beyond those suggested by *sp* truncation and M_{1+} dominance. Most notably, R^n_{L+T} and R^ℓ_{TT} display significant curvature throughout the central W region where the statistical precision is sufficient to reject the linear behavior of the *sp* truncation. However, the angular coverage for $W \geq 1.31$ or $W \leq 1.19$ GeV is not sufficient to determine the quadratic coeffcient convincingly; hence, in these outer W regions the black curves are limited to linear fits. In the outer W regions the blue curves (Fit B), which for those response functions are still quadratic fits, emerge from beneath the black curves but are poorly constrained by the available data. Similarly, the good statistical precision of the differential cross section permits extraction of quadratic contributions to R_{LT} and linear contributions to R_{TT} for $1.21 \leq W \leq 1.27$ GeV, but better out-of-plane coverage would be needed to extract those coefficients over a broader range of W. There is also some, albeit weaker, evidence for a quadratic contribution to R'_{LT} for central W. Most of the other response functions are reproduced well for $W \leq 1.29$ GeV using the *sp* truncation, but for larger W it sometimes becomes necessary to reduce the number of fitted terms below the *sp* truncation. Most notably, R'^ℓ_{TT} is cubic even in *sp* truncation but the data cannot support that many terms for $W \geq 1.31$ GeV.

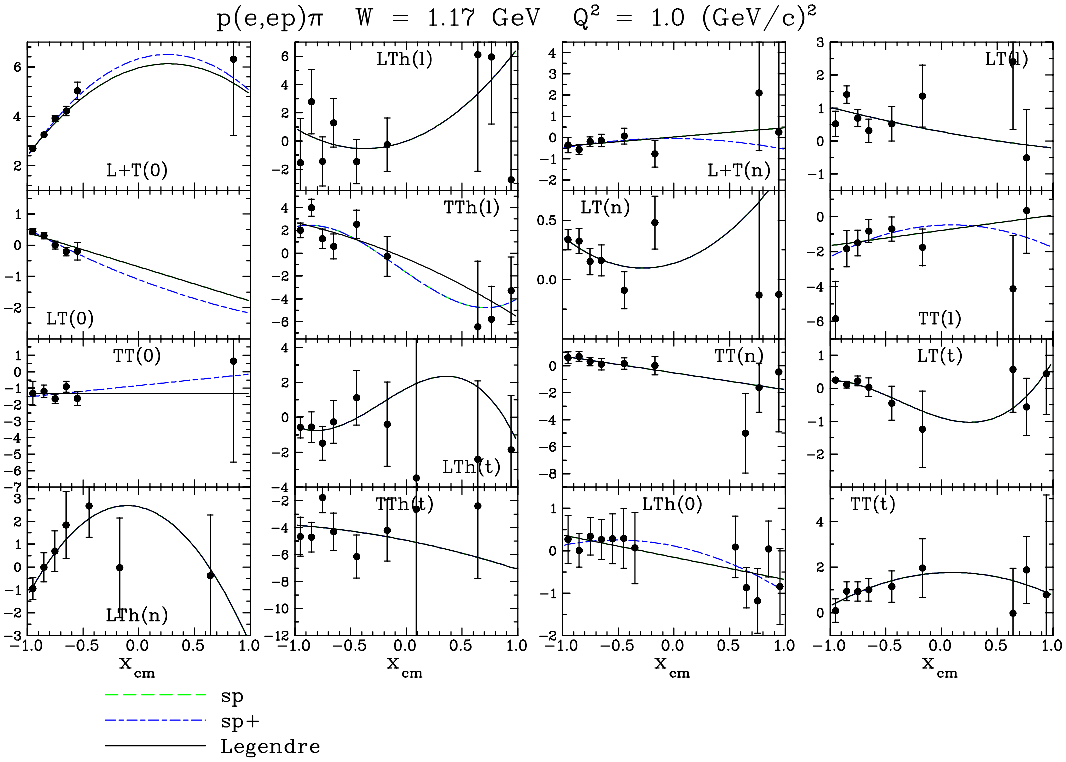

FIG. 11: Legendre fits for $W = 1.17$ GeV at $Q^2 = 1.0$ $(\mathrm{GeV}/c)^2$. Fits A, B, and C are shown as green dashed, blue dash-dot, and black curves, respectively. The units are μb and the response functions are labeled according to Tables I-III. See text for further details.

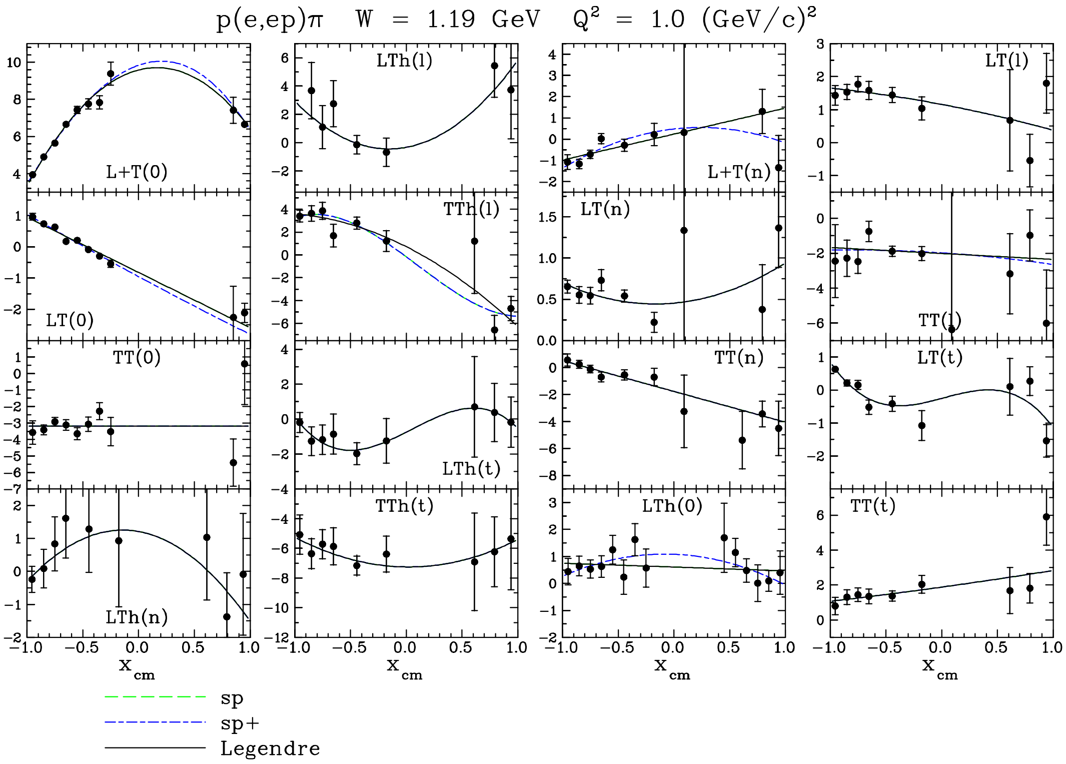

FIG. 12: Legendre fits for $W = 1.19$ GeV at $Q^2 = 1.0$ $(\mathrm{GeV}/c)^2$. See Fig. 11 for the legend.

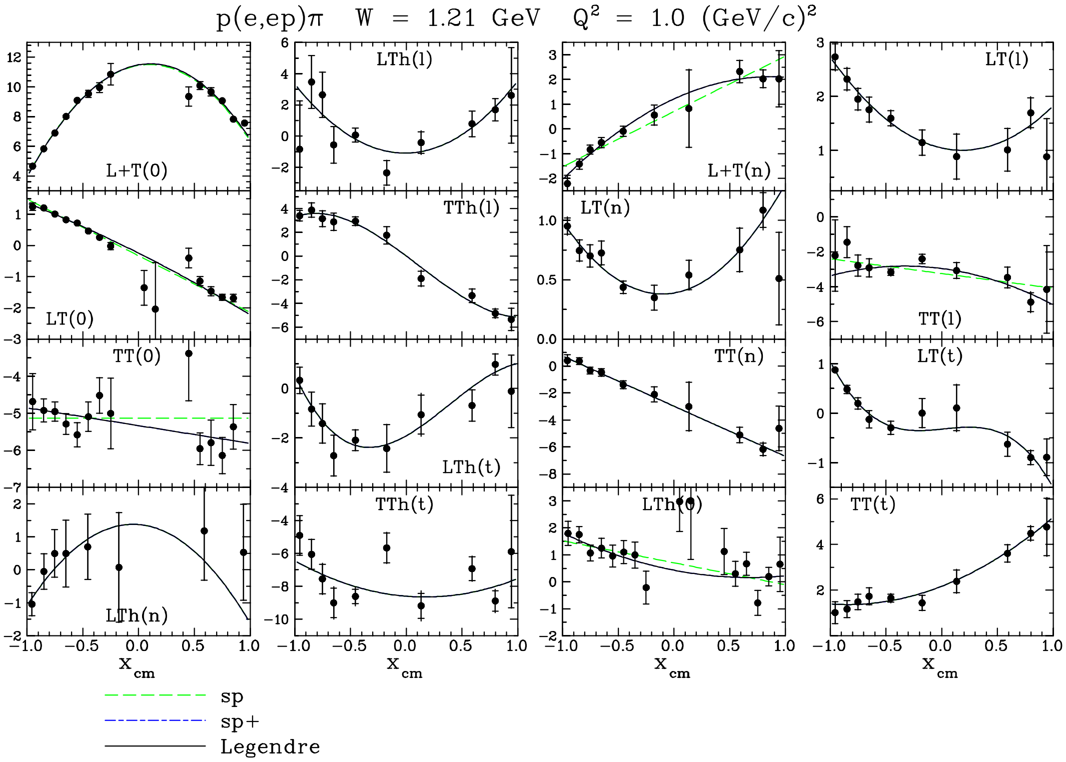

FIG. 13: Legendre fits for $W = 1.21$ GeV at $Q^2 = 1.0$ (GeV/c)^2. See Fig. 11 for the legend.

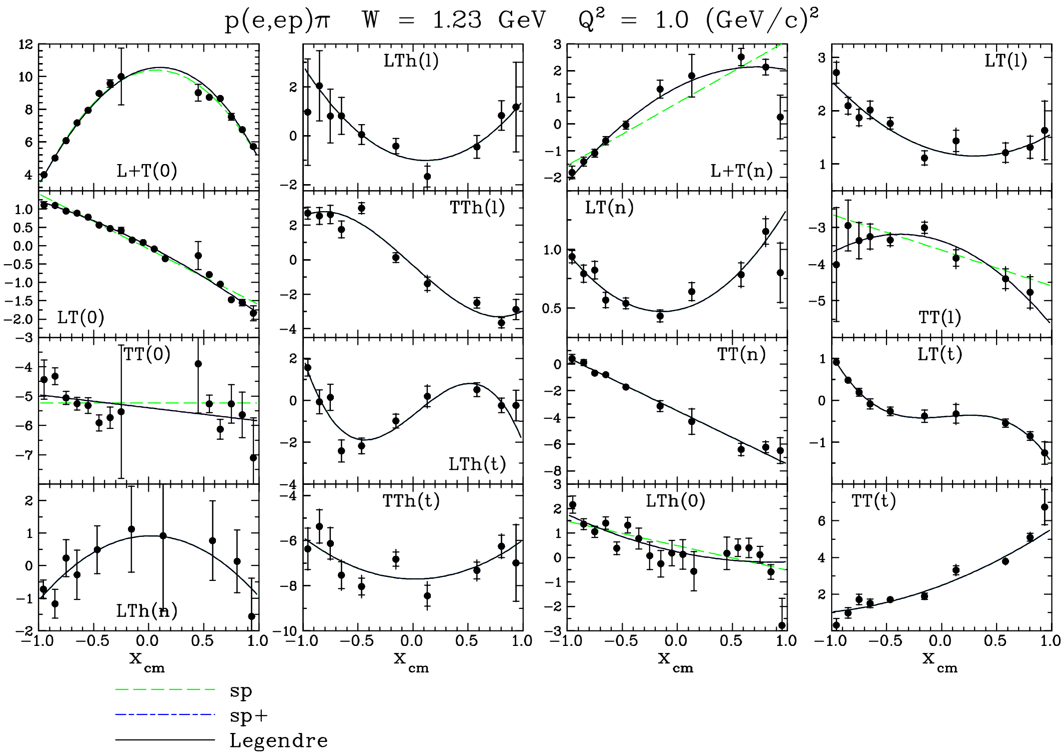

FIG. 14: Legendre fits for $W = 1.23$ GeV at $Q^2 = 1.0$ (GeV/c)^2. See Fig. 11 for the legend.

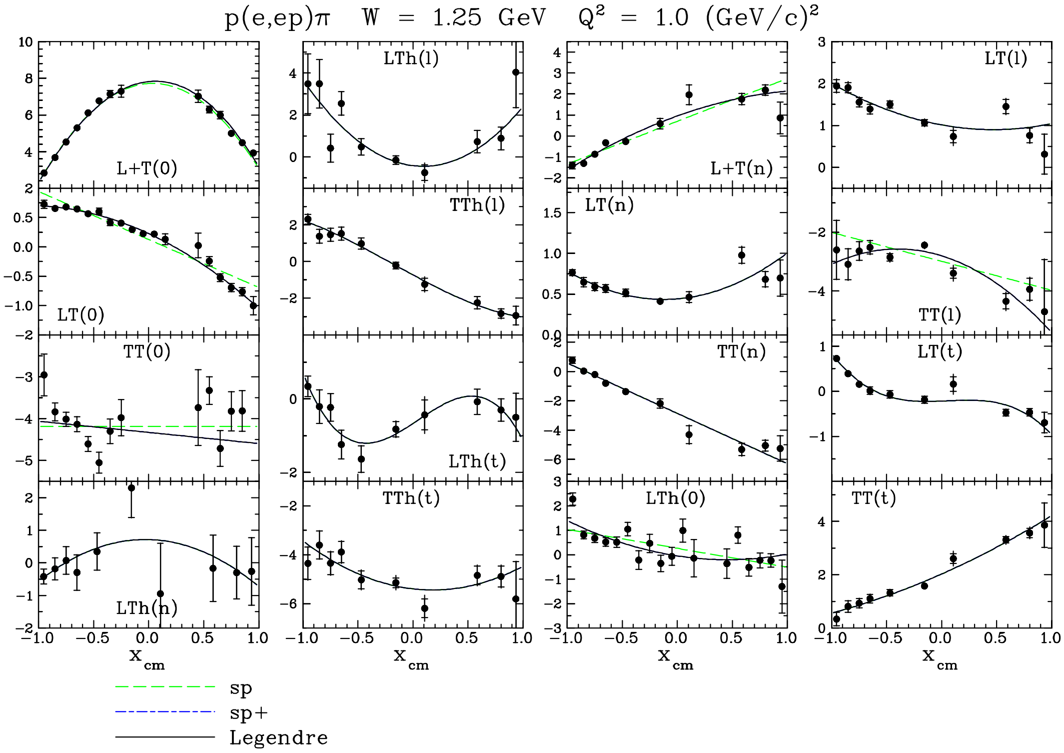

FIG. 15: Legendre fits for $W = 1.25$ GeV at $Q^2 = 1.0$ (GeV/c)^2. See Fig. 11 for the legend.

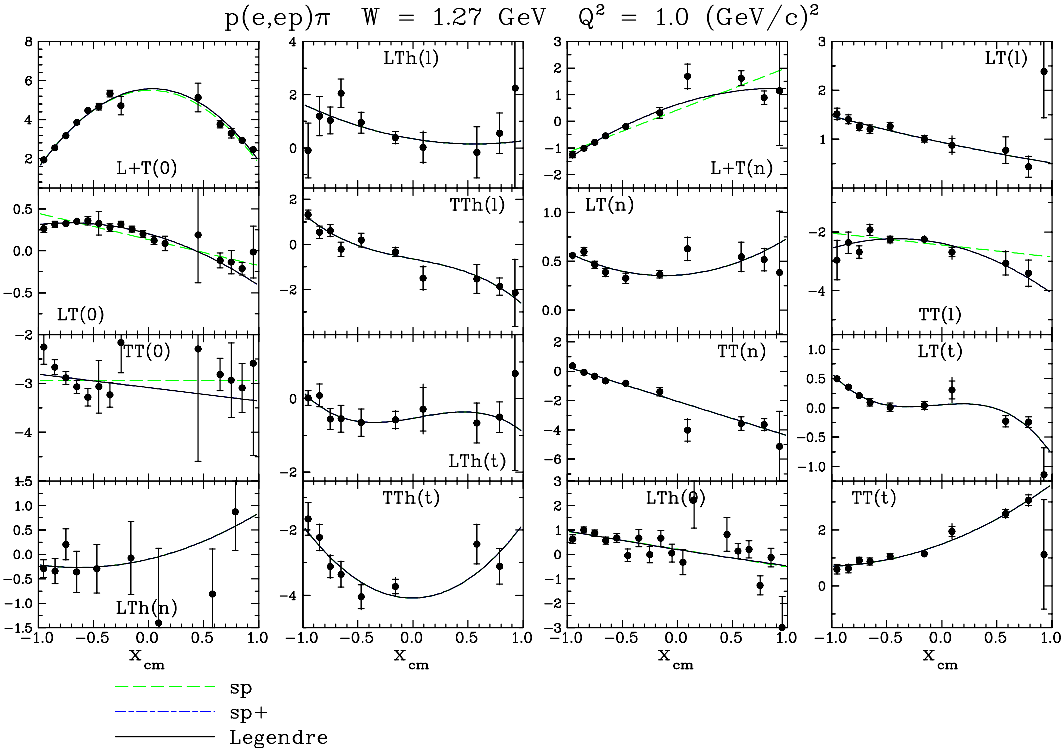

FIG. 16: Legendre fits for $W = 1.27$ GeV at $Q^2 = 1.0$ (GeV/c)^2. See Fig. 11 for the legend.

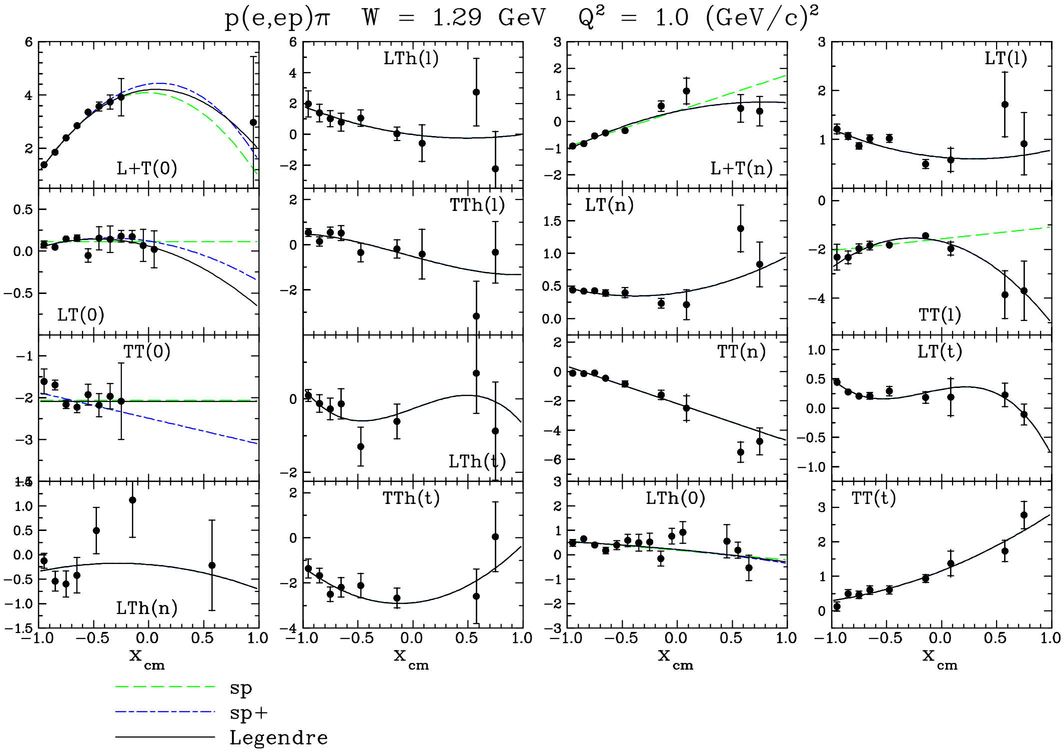

FIG. 17: Legendre fits for $W = 1.29$ GeV at $Q^2 = 1.0$ (GeV$/c)^2$. See Fig. 11 for the legend.

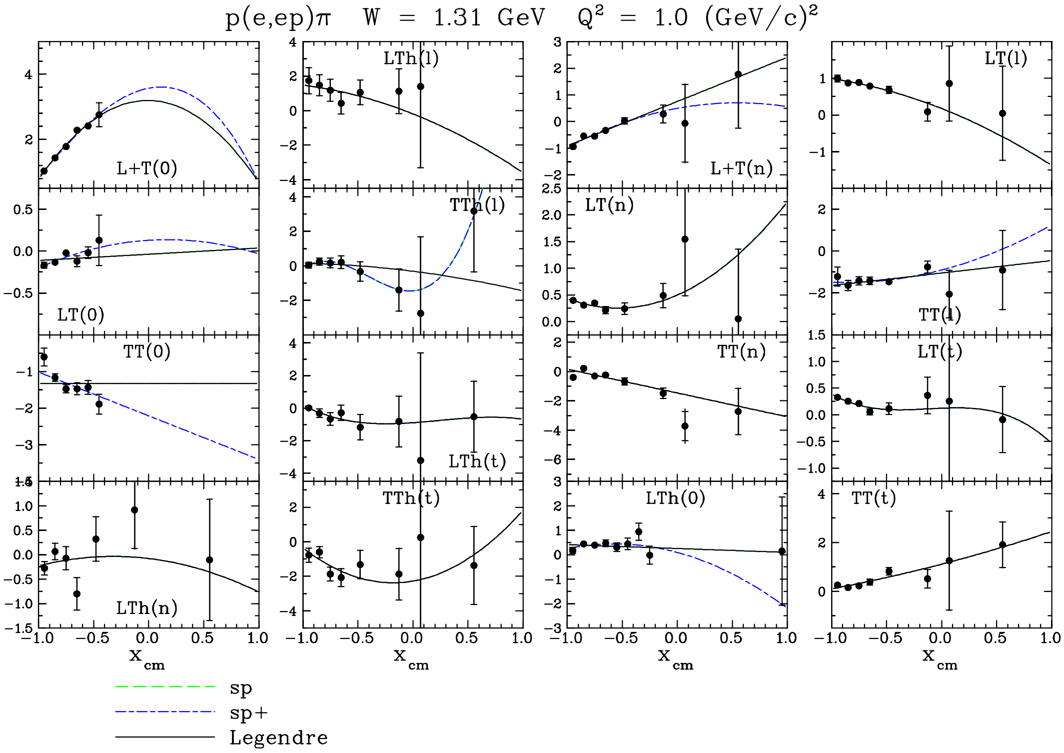

FIG. 18: Legendre fits for $W = 1.31$ GeV at $Q^2 = 1.0$ (GeV$/c)^2$. See Fig. 11 for the legend.

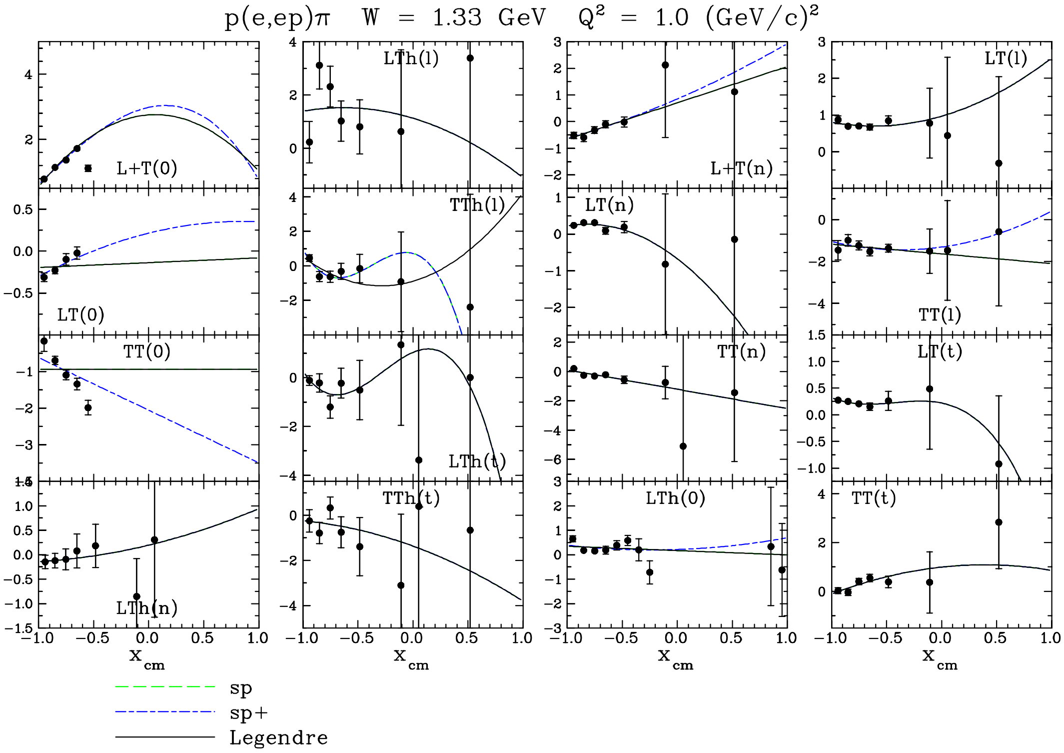

FIG. 19: Legendre fits for $W = 1.33$ GeV at $Q^2 = 1.0$ (GeV/c)^2. See Fig. 11 for the legend.

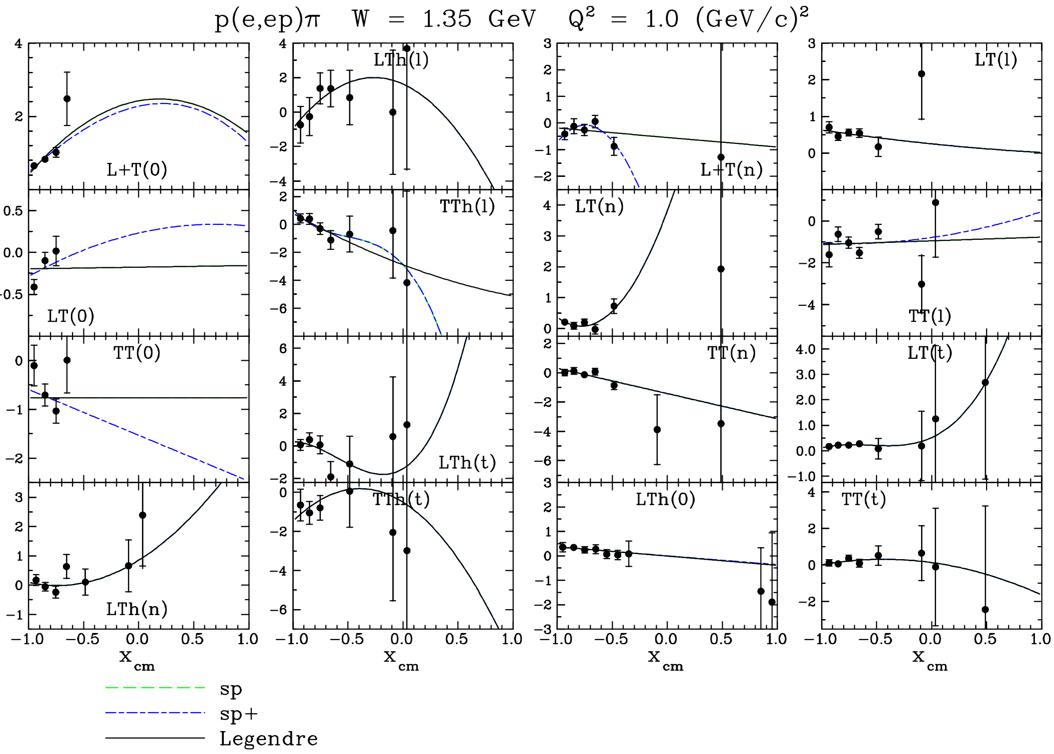

FIG. 20: Legendre fits for $W = 1.35$ GeV at $Q^2 = 1.0$ (GeV/c)^2. See Fig. 11 for the legend.

C. Legendre coefficients

Figures 21-28 compare fitted Legendre coefficients obtained using the three truncation schemes. Open green circles show Fit A (the *sp* truncation), blue diamonds show Fit B with extra terms independent of W, and filled black circles show Fit C for which the number of free parameters was optimized for each W. The best results are obviously obtained in the central region, $1.21 \leq W \leq 1.29$ GeV, where the angular coverage is the most complete, but useful information is obtained for many of the coefficients on both sides of the central region also. The largest error bars are obtained for Fit B because it has the greatest number of free parameters, often more than the data can constrain. The smallest errors bars are obtained for Fit A, except for those few cases in which Fit C varied fewer terms than Fit A, In most cases we find that inclusion of one or two extra terms has relatively little effect upon results for lower coefficients. For Fit C inner error bars with endcaps show statistical uncertainties while outer error bars without endcaps show total uncertainties with systematic errors added in quadrature; however, the systematic contributions are usually smaller than statistical uncertainties and are rarely visible.

Figures 21-28 also compare fitted Legendre coefficients with calculations for $Q^2 = 1.0$ (GeV$/c)^2$ based upon the MAID2003 [2], DMT [10], SL [9], and SAID [11] models. Model calculations for Legendre coefficients beyond *sp* truncation sometimes exhibit nodes near $W = 1.23$ GeV, but that behavior is hardly guaranteed — some of the higher-order terms actually peak near $W = 1.23$ GeV. Therefore, although the models can provide some useful guidance, the appropriate truncation must be decided for each response function based upon the data.

The statistical precision of the differential cross section data is sufficient to seek an additional term in each of the R_{L+T}, R_{LT}, and R_{TT} response functions, at least in the central W region. We find that the cubic contribution to R_{L+T} is quite small, consistent with most model calculations. However, A_1^{L+T} is appreciably stronger than MAID, DMT, or SL predictions and exhibits an upturn for $W \gtrsim 1.3$ GeV that is absent from those models. This result is not affected by the inclusion of terms beyond *sp* truncation. The models reproduce the even $L+T$ coefficients relatively well, although the W dependence of the SAID calculation for A_2^{L+T} is somewhat too flat. Similarly, the models describe A_0^{TT} well. The fitted linear TT term for central W is consistent in both sign and magnitude with model calculations. For R_{LT} we find a significant quadratic term that is consistent with MAID and DMT predictions but somewhat at variance with the the other two curves. The inclusion of this term in the fit does not adversely affect the lower coefficients; in fact, it appears that reasonable results are obtained for A_2^{LT} over a broad range of W even though their uncertainties are larger outside the central region. However, extra terms do increase uncertainties for lower coeffcients even if fitted values are not strongly affected.

The beam analyzing power data also provide an additional coefficient beyond *sp* in the central W region without adverse effects upon lower coefficients. The fitted A_2^{LTh} is consistent with model predictions, but the spread among A_0^{LTh} calculations is rather large and none of the calculations provides a good description of the W dependence for that coefficient. We could also obtain a quadratic contribution to R_{TT}^{ℓ} in the central region, with a coefficient that is somewhat stronger than MAID, DMT, or SL models; however, it appears that the *sp* truncation may be more reliable for $W = 1.29$ GeV. Interestingly, the sign of the SAID prediction for $A_2^{TT\ell}$ is opposite that of the data over most of this W range. Similarly, although the spread among R_{L+T}^{n} calculations is also rather large, MAID provides the best overall fit to the data for its Legendre coefficients, including the quadratic term in the central region.

It is not possible to extract an extra term from these R_{LT}^{ℓ} data; even the highest *sp* term becomes problematical outside the central W region. The variation among model calculations for $A_1^{LT\ell}$ is striking, but none reproduces the data.

The models describe the Legendre coefficients for R_{TT}^{t} relatively well, but none of them describes the set of coefficients for R_{LT}^{t}. Similarly, the models are more successful for R_{TT}^{n} than for R_{LT}^{n}, where both MAID and DMT get the wrong sign for the linear term and SAID is much too large. The models are generally more successful for the helicity-dependent response functions, although SAID often stands out.

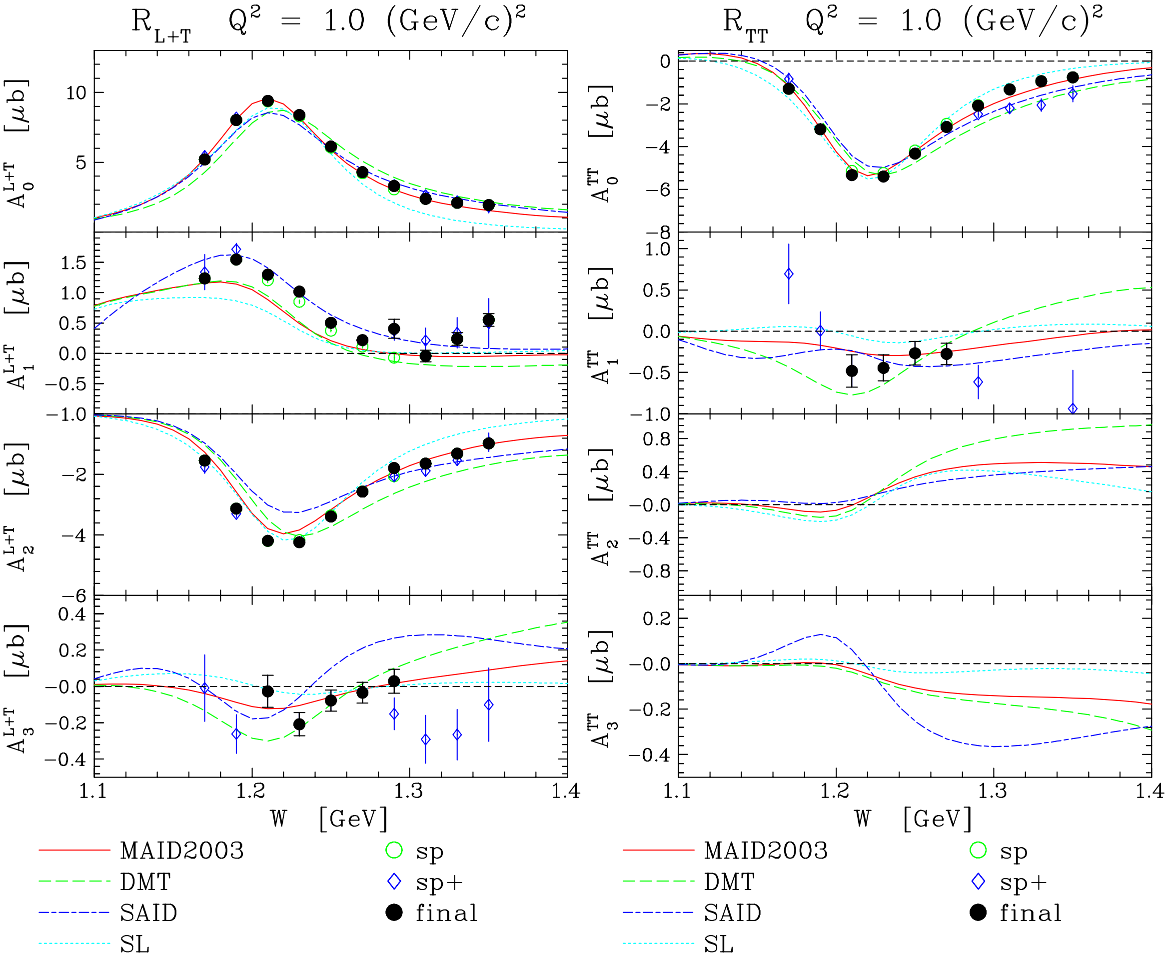

FIG. 21: Legendre coefficients for $Q^2 = 1.0$ (GeV/c)^2.

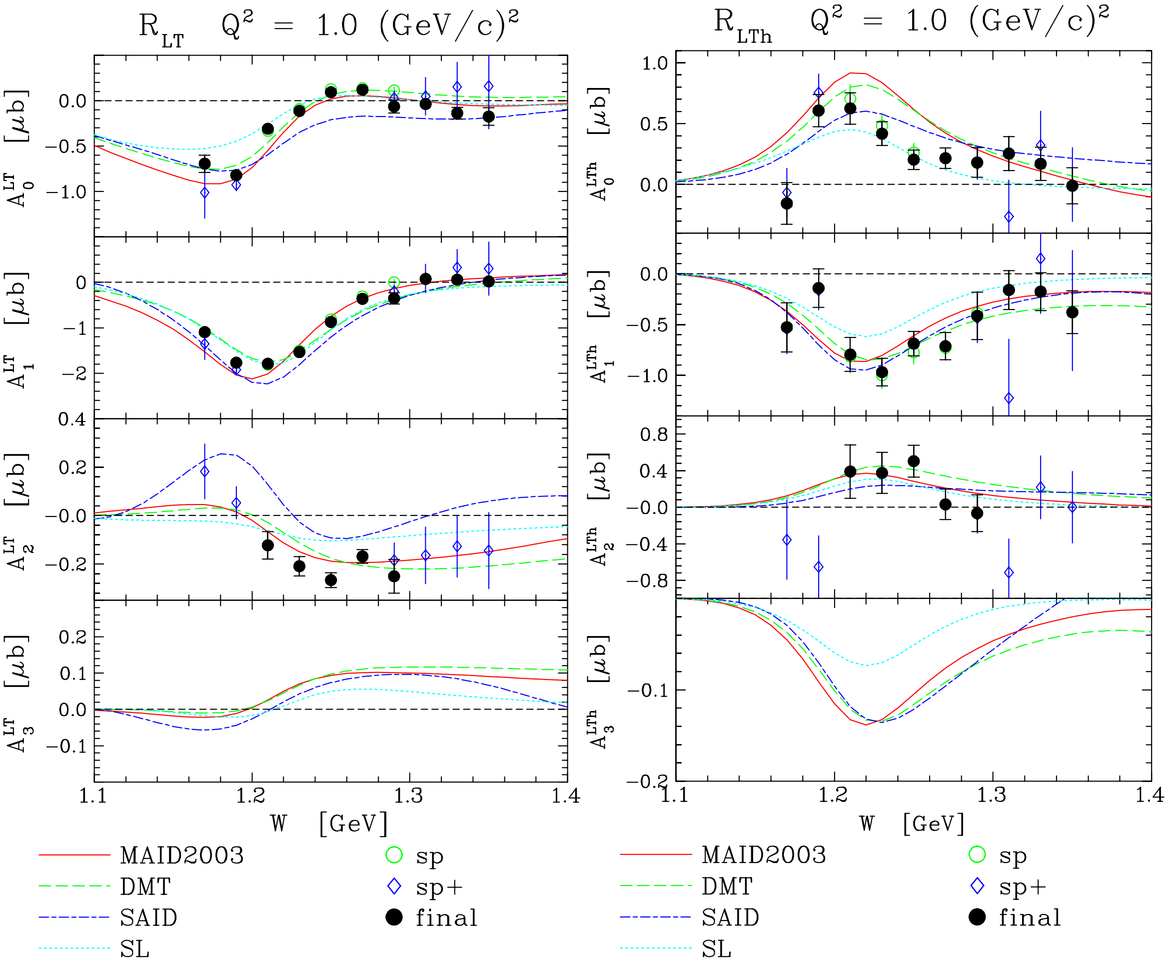

FIG. 22: Legendre coefficients for $Q^2 = 1.0$ (GeV/c)^2.

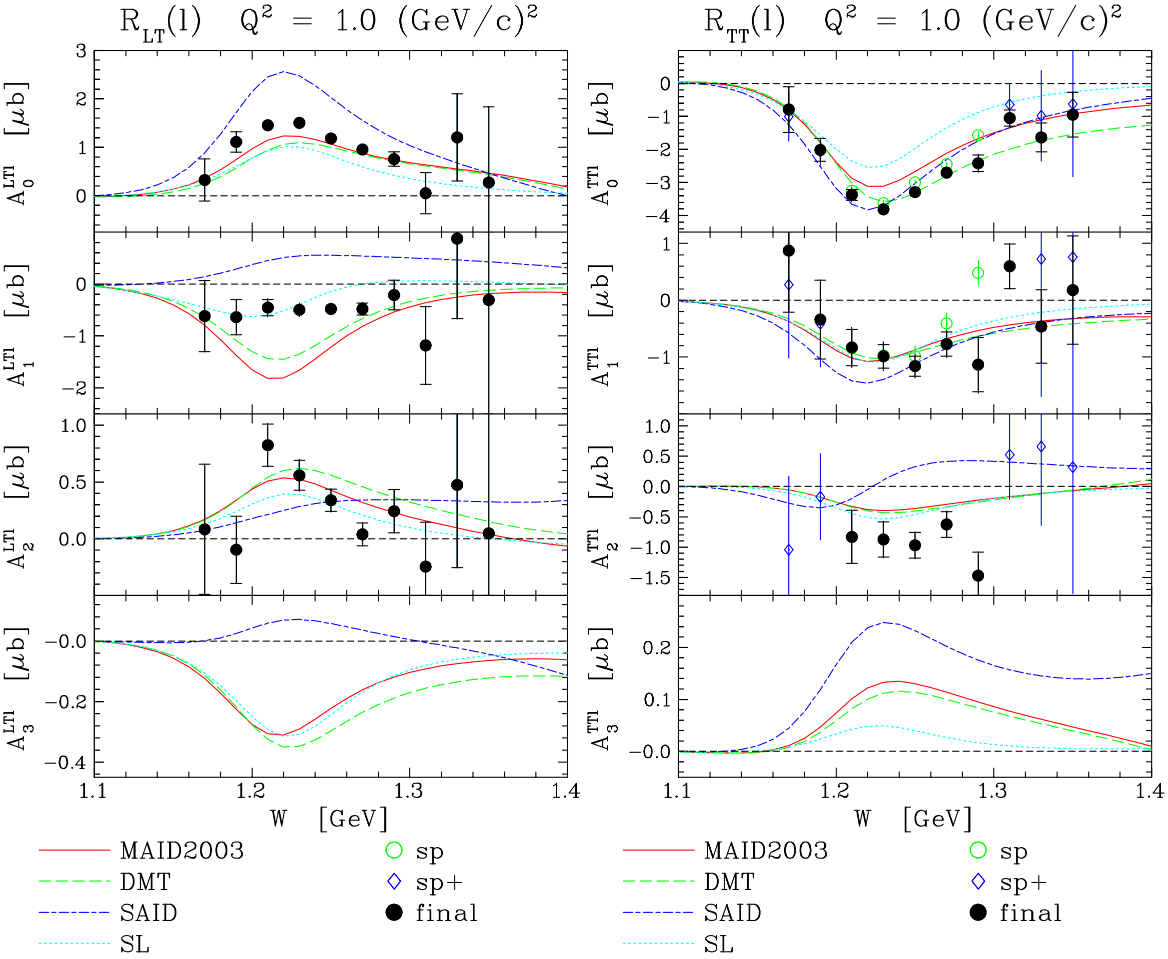

FIG. 23: Legendre coefficients for $Q^2 = 1.0$ $(\mathrm{GeV}/c)^2$.

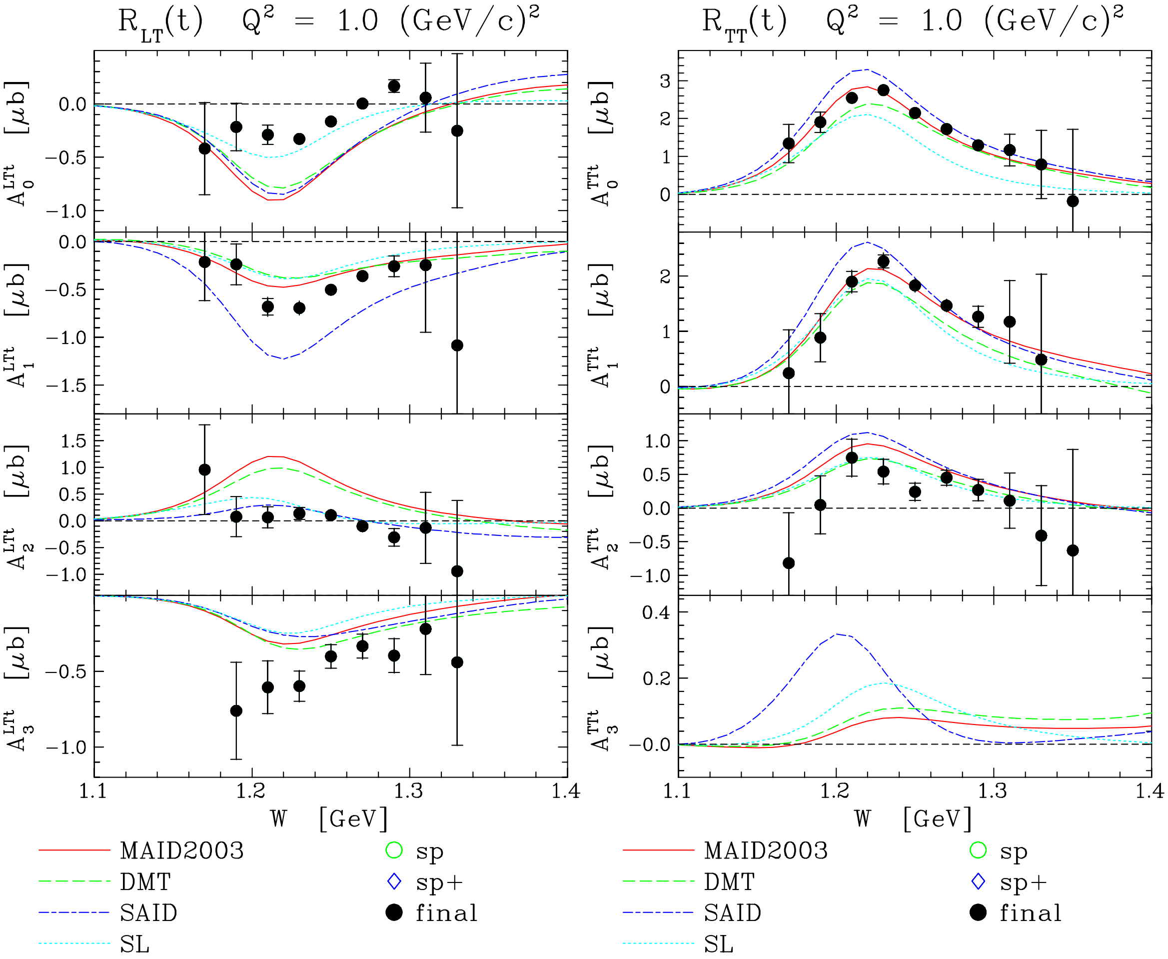

FIG. 24: Legendre coefficients for $Q^2 = 1.0$ (GeV/c)^2.

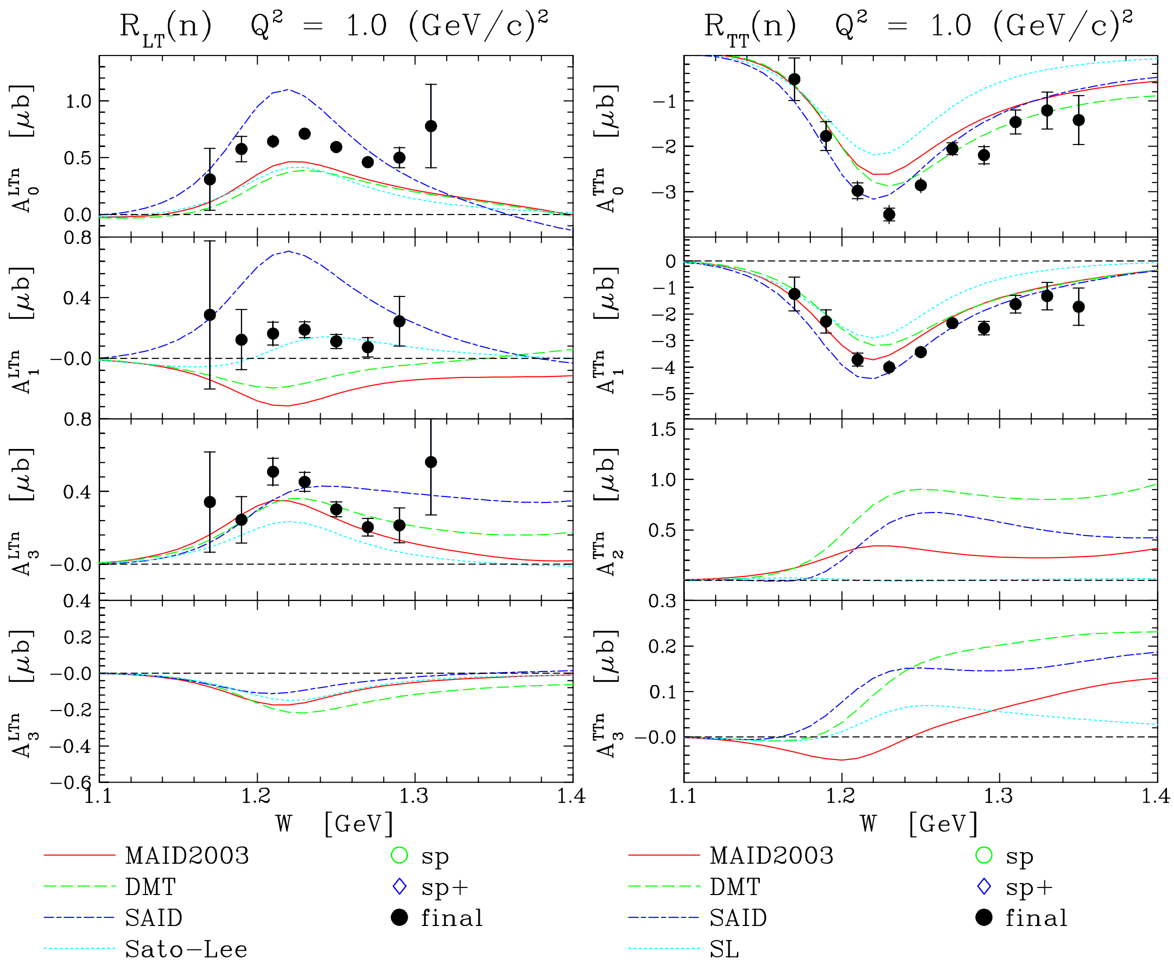

FIG. 25: Legendre coefficients for $Q^2 = 1.0$ (GeV$/c$)^2.

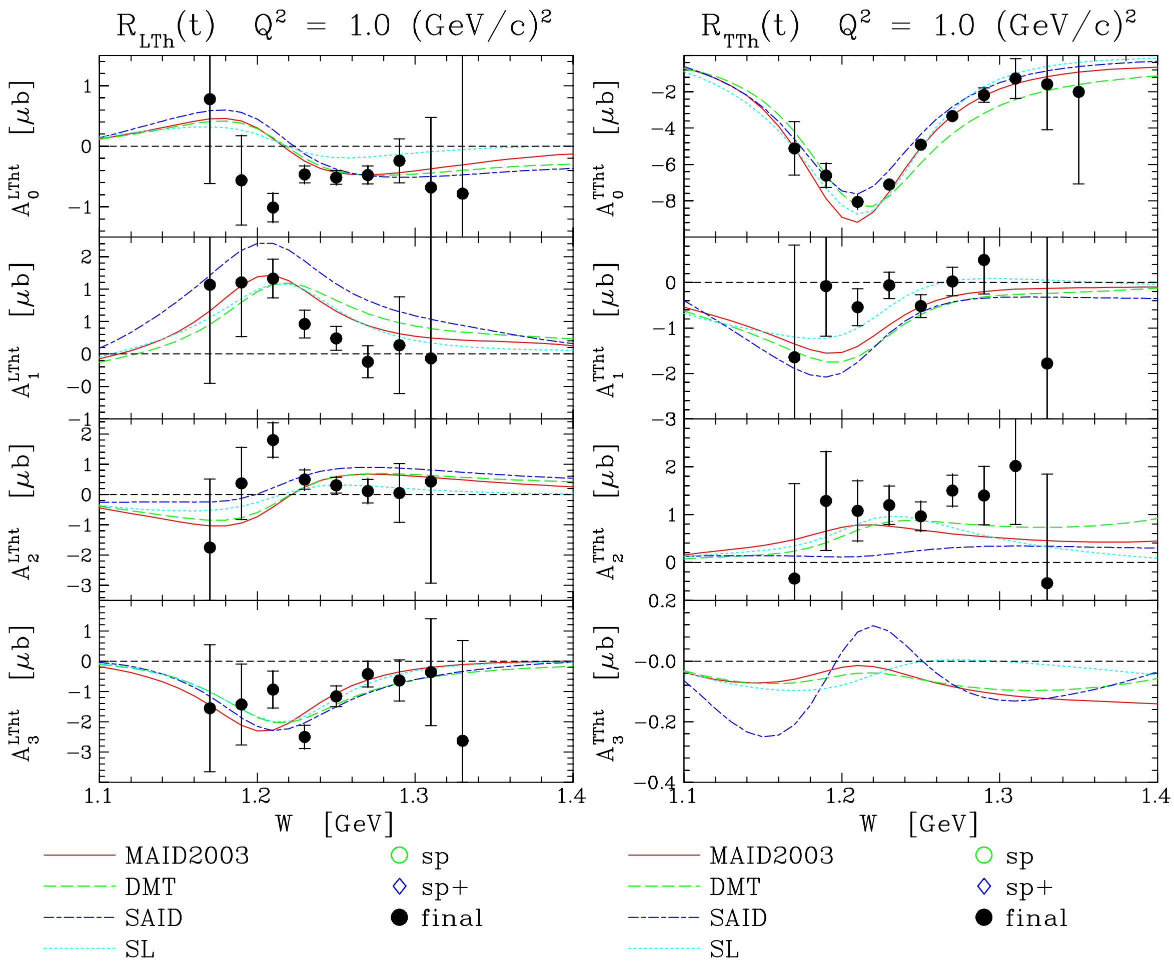

FIG. 26: Legendre coefficients for $Q^2 = 1.0$ (GeV/c)^2.

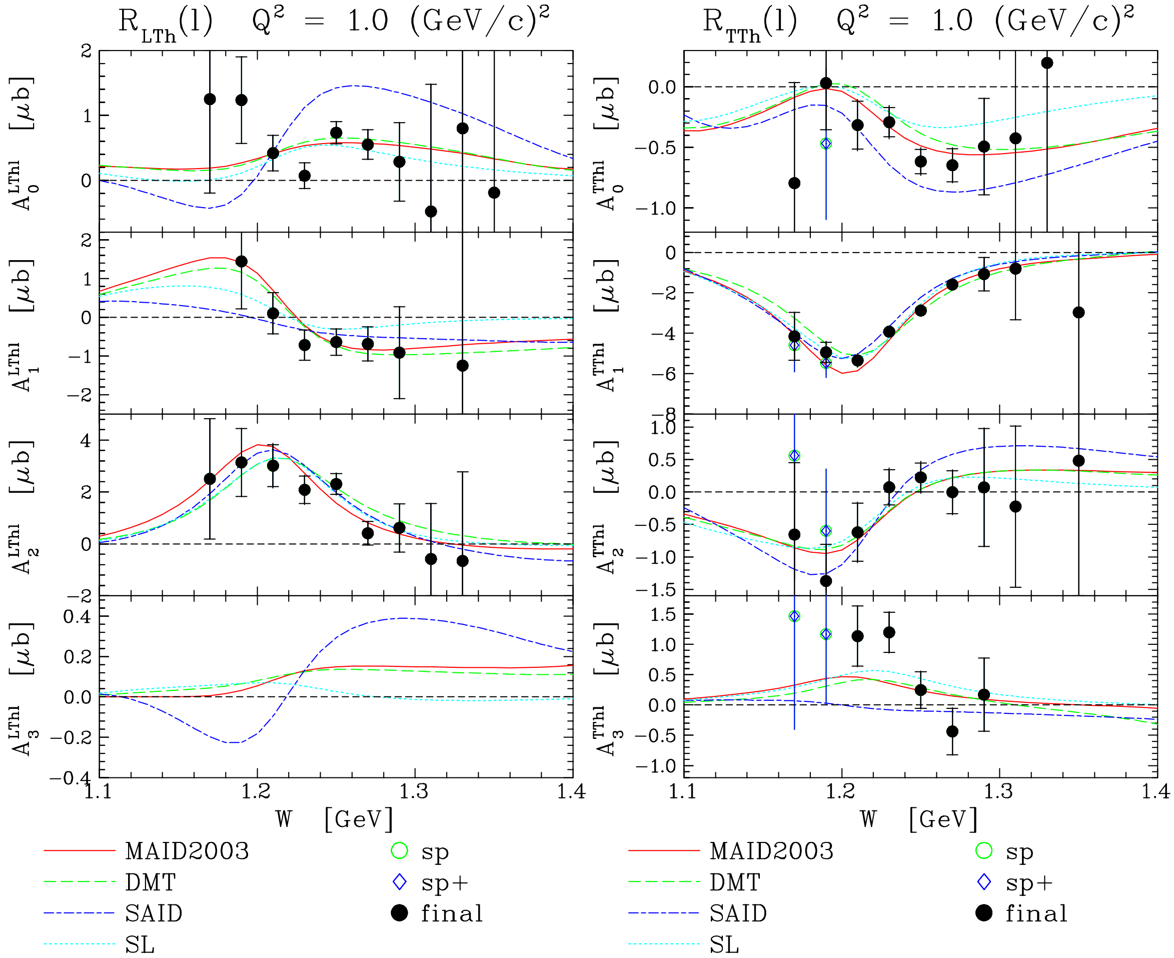

FIG. 27: Legendre coefficients for $Q^2 = 1.0$ (GeV/c)^2.

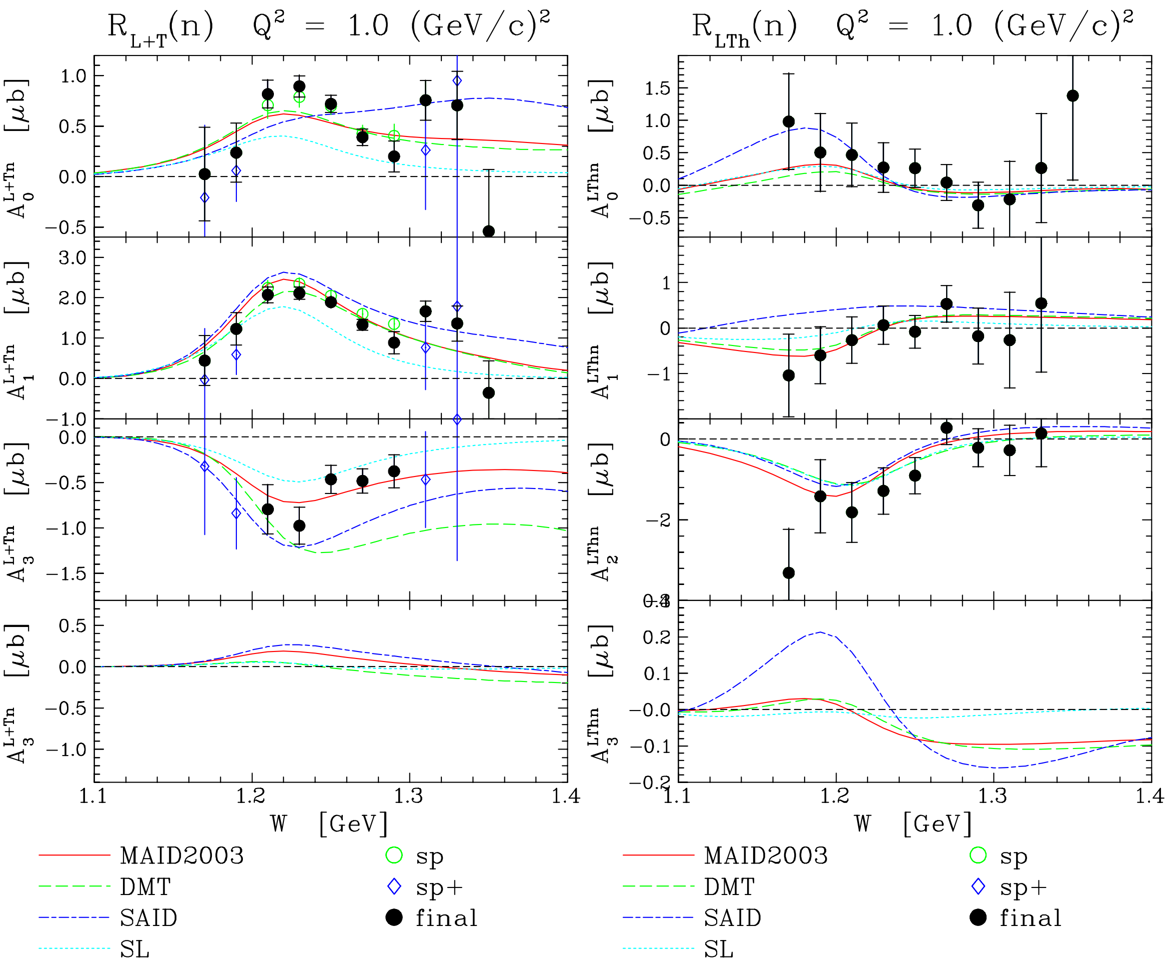

FIG. 28: Legendre coefficients for $Q^2 = 1.0$ (GeV/c)^2.

IV. COMPARISON WITH CLAS

A direct comparison between Legendre coefficients extracted by e91011 and by CLAS [12] is complicated by the differences in Q^2 binning and for R_{L+T} by variations of ϵ. The e91011 data are at $Q^2 = 1.0$ (GeV/c)^2 while the nearest bins for the CLAS data are 0.9 and 1.15. For the sake of comparison we assume that the Q^2 dependence of Legendre coefficients is described adequately by a dipole form factor and scale the CLAS data according to

$$R(Q_0^2) = R(Q^2)\left(\frac{1+Q^2/\Lambda^2}{1+Q_0^2/\Lambda^2}\right)^4 \tag{4}$$

where $\Lambda^2 = 0.71$ (GeV/c)^2 is the traditional dipole scale and where $Q_0^2 = 1.0$ (GeV/c)^2 represents central kinematics for e91011. We also consider only the higher beam energy, $E_i = 2.445$ GeV, for the CLAS experiment in order to reduce variations due to ϵ. Note, however, that for a given W, ϵ is higher for $Q^2 = 0.9$ than for 1.15 (GeV/c)^2 and that ϵ for e91011 is higher than for either of the CLAS data sets.

Legendre coefficients for unpolarized response functions are compared in Fig. 29. We observe good qualitative agreement between these data sets, but there are significant differences in detail. For example, A_2^{L+T} is systematically stronger for low W in e91011 than in CLAS data. Nor does the form-factor scaling prescription bring the two CLAS data sets for LT coefficients into agreement with each other, but the higher Q^2 data also appear to show more scatter. On the other hand, the curvature we see in the x_{cm} dependence of R_{LT} clearly requires at least one term beyond *sp* truncation. Perhaps the omission of A_2^{LT} from the CLAS analysis is partly responsible for discrepancies in the lower coefficients.

There is also a systematic tendency for coefficients based upon the data for 1.15 (GeV/c)^2 to be stronger than those from the 0.90 (GeV/c)^2 data, which suggests that the form-factor scaling adjusts those data sets too strongly. However, because the $N \to \Delta$ form factor is steeper than the dipole form factor, we would expect the best form factor to be somewhere between the nonresonant dipole and the steeper resonance form factor. Unfortunately, the e91011 data do not have sufficient kinematic acceptance to independently evaluate the Q^2 dependencies of recoil-polarization response functions near the central value of $Q^2 = 1.0$ (GeV/c)^2. Early analyses of the e91011 experiment did attempt to obtain data for $Q^2 = 0.9$ and 1.1 (GeV/c)^2 in 5 bins of W, but the acceptance averaged $\overline{Q^2}$ varies strongly with x_{cm} and tends to be skewed toward the central value of 1.0 (GeV/c)^2. Thus, compensation for the x_{cm} dependence of $\overline{Q^2}$ requires a model and interferes with the intended test of that Q^2 dependence. Furthermore, the W dependence is more important for the Δ region than the Q^2 dependence and is smoother and more complete in the 10×1 binning scheme. Therefore, we will focus on the $Q^2 = 1.0$ (GeV/c)^2 data henceforth and discontinue the 5×2 analysis. To avoid model bias, we will use dipole scaling to compensate for small variations of $\overline{Q^2}$ with respect to x_{cm}. The effect of such variations on fitted Legendre or multipole coefficients should be much smaller than the differences between the two CLAS data sets shown in Fig. 29 because those variations tend to average out when fitting the x_{cm} dependence and the $\overline{Q^2} - Q_0^2$ differences in the e91011 data are much smaller than the difference between the two Q^2 sets compared in that figure anyway.

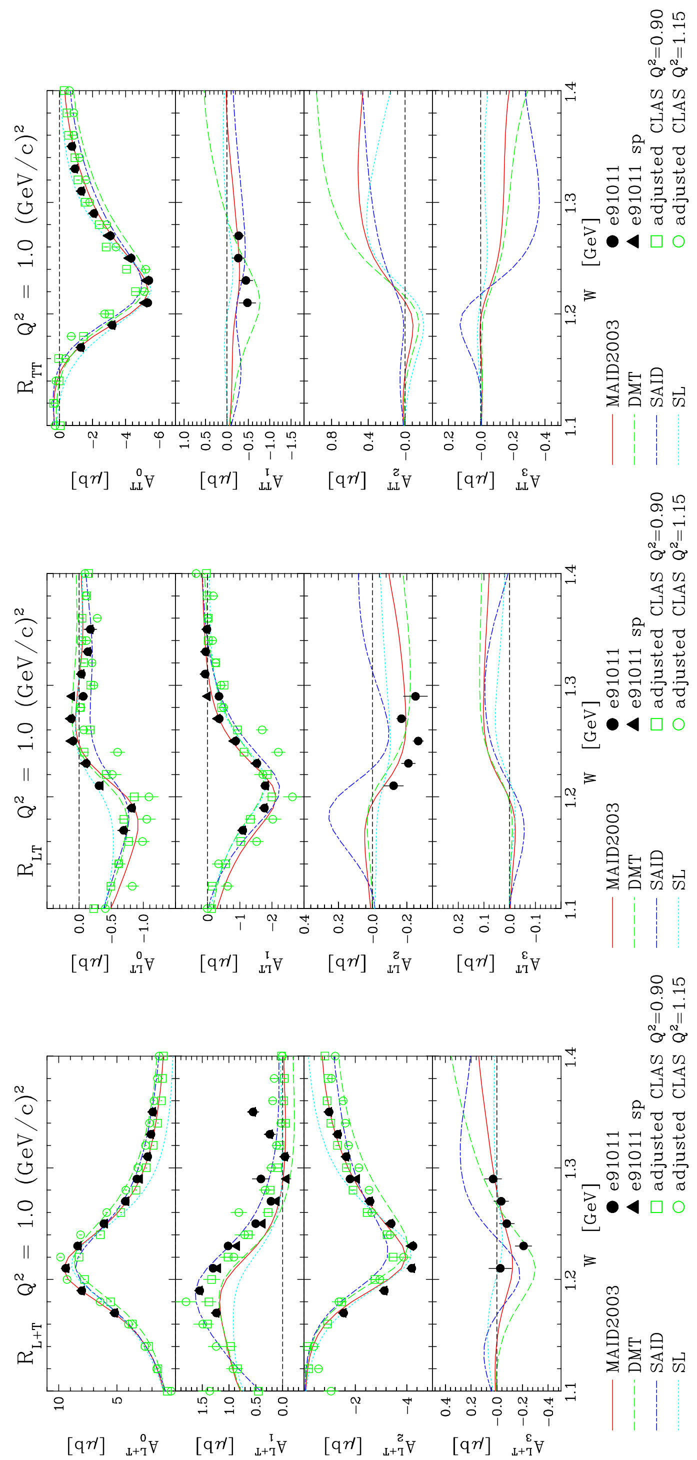

FIG. 29: Legendre coefficients for $Q^2 = 1.0$ (GeV$/c)^2$.

TABLE IV: Calculated quadrupole ratios for $W = 1.23$ GeV at $Q^2 = 1.0$ (GeV/c)^2.

model	$R_{SM}^{(p\pi^0)}$, %	$\tilde{R}_{SM}^{(p\pi^0)}$, %	$R_{EM}^{(p\pi^0)}$, %	$\tilde{R}_{EM}^{(p\pi^0)}$, %
MAID2003	−6.73	−5.63	−1.65	−1.12
DMT	−7.21	−6.10	−1.77	−1.47
SAID	−8.71	−7.88	+0.17	+0.22
SL	−6.59	−6.58	−2.29	−1.58

A. Quadrupole ratios

Most previous extractions of $R_{EM}^{(3/2)}$ and $R_{SM}^{(3/2)}$ employed truncated Legendre analysis of the unpolarized differential cross section. To the extent that M_{1+} dominance and *sp* truncation apply for $W \approx M_\Delta$, one can define

$$R_{EM}^{(p\pi^0)} \approx \tilde{R}_{EM}^{(p\pi^0)}(M_\Delta) \qquad R_{SM}^{(p\pi^0)} \approx \tilde{R}_{SM}^{(p\pi^0)}(M_\Delta) \tag{5}$$

where

$$\tilde{R}_{EM} = \frac{3A_2^{L+T} - 2A_0^{TT}}{12A_0^{L+T}} \tag{6a}$$

$$\tilde{R}_{SM} = \frac{A_1^{LT}}{3A_0^{L+T}} \tag{6b}$$

are W-dependent combinations of Legendre coefficients for a particular charge state. To obtain the desired quantities for isospin-3/2 one needs to correct for the isospin-1/2 contamination of the $p\pi^0$ channel, but that correction is expected to be small and has not been made.

Table IV compares ratios of multipole amplitudes at $W = 1.23$ GeV for several models with the corresponding truncated Legendre approximations. Obviously, the truncated Legendre approximation is not especially accurate even near M_Δ. Nevertheless, it is useful to compare data and model calculations for Legendre coefficients using Eq. (6) for both even though those formulas deviate from the corresponding multipole ratios.

Figure 30 compares calculations of $\tilde{R}_{EM}^{(p\pi^0)}(W)$ and $\tilde{R}_{SM}^{(p\pi^0)}(W)$, labeled EMR and SMR, based upon Eq. (6). Although these quantities approximate $R_{EM}^{(p\pi^0)}$ and $R_{SM}^{(p\pi^0)}$ only for $W \approx M_\Delta$, their W dependence offers some insight into the model dependence of the traditional truncated Legendre expansion. The spread among models is smallest near M_Δ, indicated by the vertical dashed line, but results for the SAID model are distinctly different from those of the MAID, DMT, or SL models. Fits A, B, and C are represented by open green circles, blue diamonds, and filled black points, respectively. In the central W region the results are practically independent of truncation scheme and in reasonable agreement with the MAID or DMT models, but for larger W the SL calculation for SMR is much flatter than the data. The positive EMR values for SAID near M_Δ disagree sharply with the data. Although it is more difficult to obtain unambiguous EMR results for $W \geq 1.31$ GeV, data based upon the *sp* truncation remain in reasonable agreement with model calculations based upon the same truncation scheme.

The results for $W \approx M_\Delta$ are listed in Table V and are practically independent of truncation scheme — the slight variation in EMR is within the estimated statistical uncertainty. We also list the values obtained by Joo *et al.* [12] using the *sp* truncation, averaging with respect to Q^2. Their results are consistent with ours for $\tilde{R}_{EM}^{(p\pi^0)}$ but are significantly larger for $\tilde{R}_{SM}^{(p\pi^0)}$. Note that Joo *et al.* estimated that truncation errors in determination of quadrupole ratios were no more than 0.5% for SMR or 0.7% for EMR in absolute terms. While we agree that truncation of Legendre fits to the number of terms in the *sp* model has little effect upon fitted values for $\tilde{R}_{EM}$ or $\tilde{R}_{SM}$, Table IV shows that deviations from R_{EM} or R_{SM} can be significantly larger. The deviations are often large for R_{SM} in absolute terms or for R_{EM} in relative terms. A more detailed analysis [13] shows that both assumptions of the traditional Legendre analysis, M_{1+} dominance and $\ell_\pi \leq 1$, are at fault. Therefore, a more rigorous analysis based upon multipole fits that do not assume *sp* truncation or M_{1+} dominance is made in Ref. [4].

TABLE V: Quadrupole ratios for $W = 1.23$ GeV at $Q^2 = 1.0$ (GeV/c)^2. The reduced chisquare for the entire data set is labeled χ^2_ν while the chisquare per point for differential cross section data is labeled $\chi^2_N(\sigma)$.

method	SMR, %	EMR, %	χ^2_ν	$\chi^2_N(\sigma)$
Fit A	-6.07 ± 0.11	-2.04 ± 0.13	1.7	1.6
Fit B	-6.11 ± 0.11	-1.92 ± 0.14	1.5	1.4
Fit C	-6.11 ± 0.11	-1.92 ± 0.14	1.5	1.4
Joo *et al.* [a]	-7.4 ± 0.4	-1.8 ± 0.4		

[a]Weighted average of $Q^2 = 0.9$ (GeV/c)^2 results for $E_i = 1.645$ and 2.445 GeV from [12].

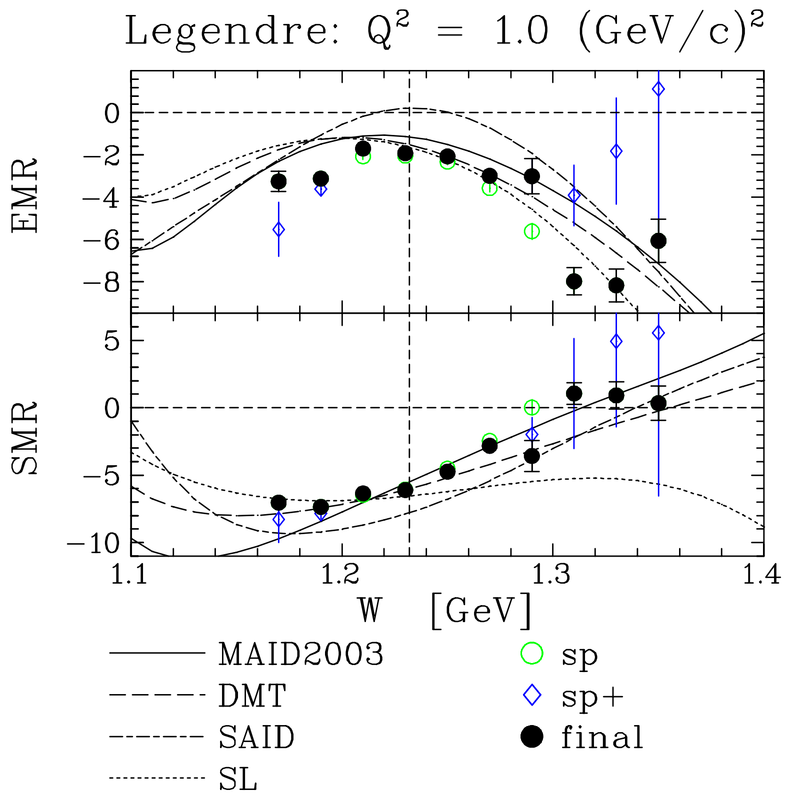

FIG. 30: Truncated Legendre approximation to quadrupole ratios. The vertical line corresponds to $W = M_\Delta$.

It is also of interest to parametrize the energy dependence of the quadrupole ratios, which facilitates interpolation to a nominal value for M_Δ. The W dependencies of multipole analyses for EMR and SMR are fit in Fig. 31 with parabolas of the form

$$y = \sum_{k=0}^{2} a_k (W - M_\Delta)^k \tag{7}$$

using a nominal value of $M_\Delta = 1.232$ GeV. The fits were confined to the central region, indicated by dotted vertical lines, where this simple parametrization should suffice for interpolation. Both fits describe the data for the central region well. The expansion coefficients are given in Table VI, where the data for quadrupole ratios are expressed in percent and where the multipole amplitudes are based upon the Born baseline. The a_0 parameters represent the best estimates of the quadrupole ratios at M_Δ but weighted linear least-squares fits with only 2 degrees of freedom do not necessarily provide realistic uncertainties. Instead, we quote the largest of $\delta R(1.23)$, δa_0, and $\delta a_0 \sqrt{\chi^2_\nu}$ where $\delta R(1.23)$ is the uncertainty in the single-energy fit to data for $W = 1.23$ GeV, δa_0 is the uncertainty in the value of a_0 according to the linear least-squares fit to the energy dependence, and χ^2_ν is the reduced chisquare for that fit in the central region. Although this method

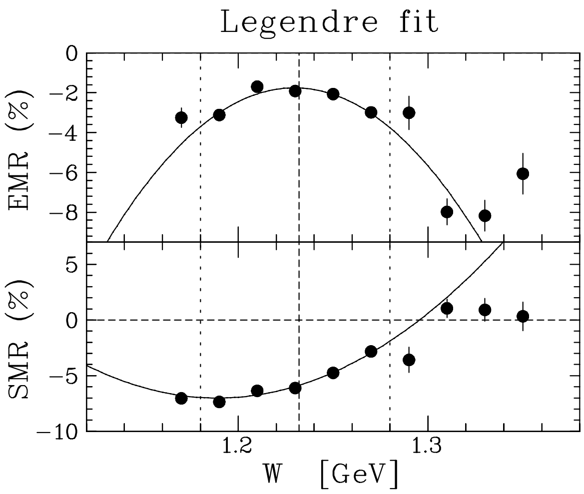

FIG. 31: Parabolic fits to the W dependence of Legendre estimators of the quadrupole ratios. Vertical dashed and dotted lines show M_Δ and the fitted ranges of W.

TABLE VI: Power series for quadrupole ratios in terms of $(W - M_\Delta)$ in units of GeV.

EMR				SMR			
a_0	a_1	a_2	χ^2_ν	a_0	a_1	a_2	χ^2_ν
-1.76 ± 0.19	-3.77	-793	2.9	-5.87 ± 0.20	53.2	618	5.2

results in larger error bars at $W = 1.232$ GeV than obtained from the single-energy fits, they are probably more realistic. The second-order terms are negligible between M_Δ and the nearest W bin and changes due to the linear terms are less than one standard deviation. For example, the fitted EMR and SMR values for the Legendre analysis are -1.75 and -5.97% at $W = 1.23$ GeV. The remaining differences between these values and those listed on the last line of Table V are less than one standard deviation. Therefore, although the quadrupole ratios in Table VI are slightly smaller than those reported in Ref. [14] using the same data, the results are consistent — the differences are partly due to variations with respect to W and partly due to statistical fluctuations of the data for 1.23 GeV relative to the average trends represented by the curves in Fig. 31.

V. CONCLUSIONS

We have fit Legendre coefficients to angular distributions of differential cross section, beam analyzing power, and recoil-polarization response functions for the $p(\vec{e}, e'\vec{p})\pi^0$ reaction at $Q^2 = 1.0$ (GeV/c)^2 across the Δ resonance. Several truncation schemes were employed. For most response functions it is sufficient to limit the number of terms according to the hypothesis of M_{1+} dominance, but good fits to the data for R_{LT}, R^n_{L+T}, and R^ℓ_{TT} require an additional term in the central W region, $1.21 \leq W \leq 1.29$ GeV. There is also weaker evidence for higher-order contributions to R_{TT} and R'_{LT}. Although retention of these extra terms has little effect on the values of lower coefficients outside the central W range, error bars tend to expand when the angular coverage is insufficient to constrain those coefficients. Therefore, the optimum fit uses fewer terms outside the central W region.

The fitted Legendre coefficients were compared with MAID2003, DMT, SL, and SAID calculations. The variation among models tends to be smallest for lower-order terms in response functions of real type that are dominated by resonant multipoles. Among these models MAID2003 provides the best overall description of the Legendre coefficients while SAID calculations sometimes have incorrect sign and rather different magnitude. However, some of the coefficients are not described well by any of the models and none provides a uniformly good fit to these data. Hopefully these data will provide valuable constraints upon future models.

We also evaluated quadrupole ratios for $N \to \Delta$ excitation based upon the traditional truncated Legendre approximation. Using parabolic fits to the energy dependence near M_Δ, we find $\tilde{R}_{SM}^{(p\pi^0)} = -5.87 \pm 0.20\%$ and $\tilde{R}_{EM}^{(p\pi^0)} = -1.76 \pm 0.19\%$ at $W = 1.232$ GeV and $Q^2 = 1.0$ (GeV/c)^2, where the error bars include both statistical and experimental systematic uncertainties. Although these quantities do not necessarily agree with the desired ratios of multipoles amplitudes, they can be compared with model calculations of the same quantities evaluated in the same manner. We find that the W dependencies for fitted combinations of Legendre coefficients are similar to corresponding calculations based upon MAID2003, DMT, or SL models but for EMR are slightly stronger at the pole position than any of these predictions. Conversely, the SAID results are stronger for SMR and opposite in sign for EMR. Our results should also be compared with the CLAS results of $-7.4 \pm 0.4\%$ and $-1.8 \pm 0.4\%$ at $Q^2 = 0.9$ (GeV/c)^2. Good agreement is obtained for EMR, but our SMR result is significantly smaller and has better statistical precision.

---

[1] J. J. Kelly *et al.*, `www.physics.umd.edu/enp/jjkelly/e91011/Reports/Publications/Drafts/ndel%ta_prc.ps.gz`, to be submitted to Phys. Rev. C (unpublished).
[2] D. Drechsel, O. Hanstein, S. S. Kamalov, L. Tiator, and S. N. Yang, `www.kph.uni-mainz.de/MAID`.
[3] Z. Chai, Ph.D. thesis, Massachusetts Institute of Technology, 2003.
[4] J. J. Kelly, `www.physics.umd.edu/enp/jjkelly/e91011/Reports/Analysis/mpamps.ps.gz` (unpublished).
[5] J. J. Kelly and O. Gayou, `www.physics.umd.edu/enp/jjkelly/e91011/Reports/Analysis/syserr.ps.gz` (unpublished).
[6] S. Escoffier, Ph.D. thesis, University of Paris, 2001.
[7] V. Punjabi *et al.*, Phys. Rev. **C 71**, 055202 (2005).
[8] L. Pentchev, JLAB-TN-03-024 (unpublished).
[9] T. Sato and T.-S. H. Lee, Phys. Rev. **C 63**, 055201 (2001).
[10] D. Drechsel, O. Hanstein, S. S. Kamalov, L. Tiator, and S. N. Yang, `www.kph.uni-mainz.de/maid/dmt`.
[11] R. A. Arndt, W. J. Briscoe, R. L. Workman, and I. I. Strakovsky, `gwdac.phys.gwu.edu`.
[12] K. Joo *et al.*, Phys. Rev. Lett. **88**, 122001 (2002).
[13] J. J. Kelly, arXiv:nucl-ex/0705010 (unpublished).
[14] J. J. Kelly *et al.*, arXiv:nucl-ex/0505024 (unpublished).
[15] Monotonic variations would induce systematic errors in Legendre coefficients without increasing scatter, but our $\overline{Q^2}$ variations are definitely nonmonotonic.